

## Review

# PET-MR and SPECT-MR multimodality probes: Development and challenges

Chang-Tong Yang<sup>1,5,6</sup>, Krishna K. Ghosh<sup>1</sup>, Parasuraman Padmanabhan<sup>1</sup>, Oliver Langer<sup>3,4</sup>, Jiang Liu<sup>5</sup>, David Ng Chee Eng<sup>6,7</sup>, Christer Halldin<sup>1,2</sup>, Balázs Gulyás<sup>1,2</sup>

1. Lee Kong Chian School of Medicine, Nanyang Technological University Singapore, 59 Nanyang Drive, Singapore 636921.
2. Karolinska Institutet, Department of Clinical Neuroscience, S-171 76, Stockholm, Sweden.
3. Department of Clinical Pharmacology and Department of Biomedical Imaging and Image-Guided Therapy, Medical University of Vienna, A-1090, Vienna, Austria.
4. Center for Health and Bioresources, Biomedical Systems, AIT Austrian Institute of Technology GmbH, Seibersdorf, Austria.
5. Cixi Institute of Biomedical Engineering, Ningbo Institute of Industrial Technology and Ningbo Institute of Materials Technology and Engineering, Chinese Academy of Sciences, Ningbo, P.R. China, 315201.
6. Department of Nuclear Medicine and Molecular Imaging, Radiological Sciences Division, Singapore General Hospital, Outram Road, Singapore 169608.
7. Duke-NUS Medical School, 8 College Road, Singapore 169857.

✉ Corresponding author: Chang-Tong Yang Email: yangct@ntu.edu.sg; yang.changtong@sgh.com.sg; chmyct@yahoo.com; Tel: (65)6326-5666.

© Ivyspring International Publisher. This is an open access article distributed under the terms of the Creative Commons Attribution (CC BY-NC) license (<https://creativecommons.org/licenses/by-nc/4.0/>). See <http://ivyspring.com/terms> for full terms and conditions.

Received: 2018.04.11; Accepted: 2018.06.08; Published: 2018.11.29

## Abstract

Positron emission tomography (PET)-magnetic resonance (MR) or single photon emission computed tomography (SPECT)-MR hybrid imaging is being used in daily clinical practice. Due to its advantages over stand-alone PET, SPECT or MR imaging, in many areas such as oncology, the demand for hybrid imaging techniques is increasing dramatically. The use of multimodal imaging probes or biomarkers in a single molecule or particle to characterize the imaging subjects such as disease tissues certainly provides us with more accurate diagnosis and promotes therapeutic accuracy. A limited number of multimodal imaging probes are being used in preclinical and potential clinical investigations. The further development of multimodal PET-MR and SPECT-MR imaging probes includes several key elements: novel synthetic strategies, high sensitivity for accurate quantification and high anatomic resolution, favourable pharmacokinetic profile and target-specific binding of a new probe. This review thoroughly summarizes all recently available and noteworthy PET-MR and SPECT-MR multimodal imaging probes including small molecule bimodal probes, nano-sized bimodal probes, small molecular trimodal probes and nano-sized trimodal probes. To the best of our knowledge, this is the first comprehensive overview of all PET-MR and SPECT-MR multimodal probes. Since the development of multimodal PET-MR and SPECT-MR imaging probes is an emerging research field, a selection of 139 papers were recognized following the literature review. The challenges for designing multimodal probes have also been addressed in order to offer some future research directions for this novel interdisciplinary research field.

Key words: bimodality imaging probe, PET-MR, SPECT-MR, contrast agent, radioligand

## Introduction

Molecular imaging can provide us with a deeper understanding of biological processes at molecular and cellular levels [1]. Molecular imaging has received considerable interest during the last few decades because of its momentous potential in diagnosis and treatment monitoring for both preclinical and clinical applications. Several molecular

imaging techniques, including optical fluorescence imaging, MRI, PET and SPECT, are extensively used nowadays [2, 3]. These non-invasive imaging modalities have various characteristics based on their underlying physical and technical principles. One single imaging modality may not be sufficient to obtain all necessary information and each single

molecular imaging technique has its own strengths and drawbacks: each may vary in spatial and temporal resolution, depth of subject penetration, detection threshold, etc. [4]. For example, optical fluorescence imaging offers high sensitivity, specificity and resolution, but it suffers from limited tissue penetration leading to limited application for quantification of the target in deep tissues within a subject [5]. Some modalities such as PET and SPECT, which have been used extensively to visualize metabolic and physiological process, offer very high sensitivity (in the pico-nano-molar range) but provide relatively poor anatomic resolution [6-8]. On the other hand, primarily anatomical imaging modalities such as MRI and CT have been used to detect anatomical structures because of their high spatial resolution, but with relatively poor sensitivity (in the millimolar range). MRI also enables high soft tissue contrast studies using it in magnetic resonance spectroscopic (MRS) and functional magnetic resonance imaging (fMRI) application modes [9-11].

A combination of two or more imaging modalities such as PET-CT or SPECT-CT can yield complementary information regarding morphology and function in preclinical and clinical applications, and thereby such type of hybrid and/or multimodalities can provide us with synergistic advantages over single modalities alone. Utilizing PET-CT hybrid imaging is an effective approach for combining physiological and morphological information in preclinical and clinical investigations [12]. However, the combined PET and CT scan may cause errors during the co-registration of images [13, 14]. Moreover, CT scans are associated with high radiation doses. By combining PET with the MR technique, the limited spatial resolution of PET or SPECT can be overcome by providing anatomical MR images, in which regions of interest can be accurately defined. Compared to CT, the MR spectroscopic technique can provide a series of biochemical and spatially localized metabolic information, and it does not require any radiation that could cause a problem in case of follow-up studies for young patients [15, 16]. The complementary information obtained from PET/SPECT and MR scans can potentially improve the detection of biomarkers and disease diagnosis. The ability to correlate the physiological information obtained from PET or SPECT images with the anatomical information obtained from MR images is an efficient method to identify and localize abnormal tissue accurately [17-19]. There are mainly two different designs for combining PET-MR: sequential and simultaneous acquisition approaches. It is exceptionally important to design a PET-MR combined system without compromising the

performance of standalone PET and MR systems. However, the technical challenges triggered by the presence of magnetic field make the combination of PET-MR modalities very challenging. The deleterious interactions caused by the high magnetic field of the MR scanner and the radiofrequency (RF) interference between the MR and PET need to be tackled.

This review gives a comprehensive overview of all noteworthy PET-MR and SPECT-MR multimodal imaging probes including small molecule Gd<sup>3+</sup>-chelate-containing bimodal probes, nano-sized bimodal, small molecular and nano-sized trimodal probes. Rather than concentrating on certain classes of bimodal imaging probes [20-23] or on one aspect of bimodal probes such as potential clinical applications [24] or nano-sized dual probes [25], the present review is going to summarize systematically all presently available PET-MR and SPECT-MR multimodal imaging probes, obtained with various synthetic methodologies, having various physicochemical properties, and showing potentials for preclinical and clinical applications. Finally, the challenges for designing multimodal probes have been addressed in order to offer some future research directions for this interdisciplinary research field.

### Small molecular bimodal probes

Gd<sup>3+</sup> chelates are the most commonly used small molecule MRI contrast agents (CAs) due to seven unpaired electrons of Gd<sup>3+</sup> in the f orbital. These Gd-based CAs are extensively studied for contrast enhancement relying on T1 relaxivity. Gd<sup>3+</sup> chelates have been incorporated into other imaging modality reporters such as PET or SPECT moieties to develop bimodal probes. Small molecular Gd<sup>3+</sup> chelates-containing bimodal imaging probes with their applications are summarized in **Table 1**. A small molecule gadolinium compound Gd-DOTA-4AMP-F was reported as a T1-weighted PET-MR imaging bimodal probe [26]. The imaging probe (**Figure 1**) is composed of two reporters: a Gd-DOTA-based MR imaging reporter, which was designed to be pH-responsive, and the PET radionuclide <sup>18</sup>F, which was attached to the organic moiety of the molecule. This pH-responsive CA is a potential biomarker of tumors [27] with a <sup>18</sup>F PET reporter to provide quantification and measurements of the concentration of the probe in the tissue of interest.

**Table 1.** Small molecular bimodal probes and their applications.

Probe	PET(SPECT) reporter	MR reporter	Applications	Ref.
Gd-DOTA-4AMP-18F	18F	Gd-DOTA	Quantitative pH imaging	26
68Ga TRAP(HMDA-[DOTA]-G d)3	68Ga	Gd-DOTA	Functional PET-MR imaging	30
[Gd-L][166Ho-L]	166Ho	Gd-DOTA	pH-mapping	31

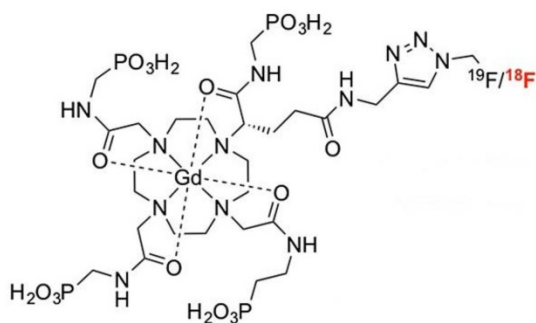


**Figure 1.** Bimodal probe Gd-DOTA-4AMP-F. Adapted with permission from [26], copyright 2010 Wiley-VCH.

Conjugates of  $Gd^{3+}$ -containing CA and additional chelators for potential PET/SPECT radiometallic ions such as  $Cu^{2+}$ ,  $Ga^{3+}$ ,  $In^{3+}$  were reported [28, 29]. The challenge lies in replacement of these radiometallic ions at a specific coordination site. Radiolabeling of responsive  $Gd^{3+}$ -containing MRI CA with  $^{68}Ga$  as small-molecular PET-MR probes  $^{68}GaTRAP(HMDA-[DOTA]-Gd)_3$  for simultaneous PET and MR acquisition was developed [30] (Figure 2). Due to its smaller macrocyclic ring compared with DOTA, the TRAP has extraordinary  $Ga^{3+}$  affinity to promote thermodynamic formation of the  $[^{68}Ga(TRAP)]$  complexes. MR signal enhancement in the functional imaging requires simultaneous mapping of CA concentration and quantitative assessment from PET data. The synthetic strategy provided a model to explore application of smart MR imaging probes for medical diagnosis through simultaneous PET-MR imaging. A dual SPECT-MRI pH-responsive probe  $[Gd-L][^{166}Ho-L]$  was developed by exchanging some of the  $Gd^{3+}$  with the SPECT radioisotope  $^{166}Ho$ . The MRI reporter and the SPECT reporter differ only in the coordinated lanthanide ion in which the SPECT reporter was used to calculate the concentration of CA for measuring the pH [31] (Figure 3).

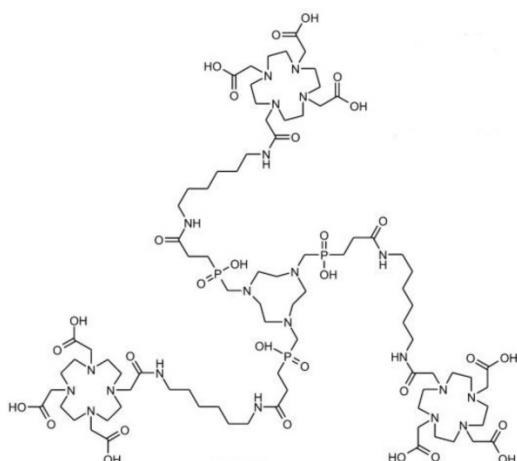


**Figure 2.** Metal complexes and  $^{68}Ga$  labeling of TRAP(HMDA-DOTA)<sub>3</sub> (1). Adapted with permission from [30], copyright 2013 Wiley-VCH.

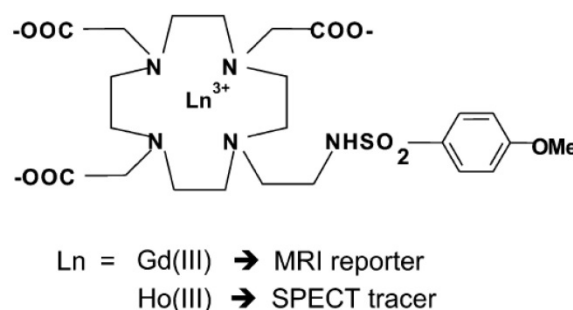


**Figure 3.** Schematic representation of the two  $Gd^{3+}$  and  $Ho^{3+}$  complexes. Adapted with permission from [31], copyright 2011 Royal Society of Chemistry.

### Nano-sized bimodal probes

Most of PET-MR and SPECT-MR bimodal imaging probes are nanoparticles or nano-sized structures because it is difficult for small molecules to carry two or more imaging reporters and even targeting groups as a single entity due to their limited loading capacity. Nano-structures have chemical and structural characteristics such as high surface area, controlled shape and size, and tuneable chemical reactivity at the surface, on coatings and inside the particle, etc. The advantages of nano-sized structures allow for carrying multimodal imaging reporters and targeting biomolecules. Approaches for development of novel multimodal PET-MR probes are mainly through surface modifications by conjugating a MR imaging reporter such as paramagnetic  $Gd^{3+}$  or superparamagnetic iron oxides (SPIOs), and by incorporating a PET radionuclide together with other functionalities. All nano-sized PET-MR and SPECT-MR bimodal imaging probes with their applications are summarized in Table 2.

A PET-MR probe  $^{64}Cu$ -DOTA-ADIO is composed of dextran sulfate-coated SPIO nanoparticles conjugated to  $^{64}Cu$ -labeled chelates [32]. This is one of the earliest scientific literature about bimodal PET-MR imaging probes. Bifunctional chelator *p*-SCN-Bz-DOTA (*S*-2(4-isothiocyanatobenzyl)-1,4,7,10-tetraazacyclododecane-1,4,7,10-tetraacetic acid) was coordinated with  $^{64}Cu$  first, which formed a thermodynamically stable chelate, then the radiolabeled chelate was conjugated to the nanoparticles. The coordination of  $^{64}Cu$  to chelator before the conjugation to nanoparticles resulted in a low yield of bimodal probe. By changing the chelator from *p*-SCN-Bz-DOTA to amine-Bz-DOTA, the radiolabeling yield increased dramatically as the linker ethylenediamine decreased the steric hindrance between the chelator and SPIO nanoparticles. A different strategy was employed for preparing radiolabeled micelle-coated SPIOs by using DOTA-conjugated phospholipids [33]. SPIOs coated with PEGylated phospholipids by hydrophobic

interaction between the capping agents on the nanoparticle surface and acyl chain of phospholipids were conjugated with DOTA-NHS-ester, then radiolabeled with  $^{64}\text{Cu}$  in the last step to achieve high yield and high purity with a hydrodynamic diameter of  $20.3 \pm 1.9$  nm (Figure 4, left). Phantom studies showed that SPIO cores in  $^{64}\text{Cu}$ -mSPIO have a dark image at high iron concentration, while a strong PET signal was observed from  $^{64}\text{Cu}$ -labeled PEG-phospholipid micelle-coated SPIO nanoparticles (Figure 4, right). As a bimodal PET-MR imaging probe, the administered dose of  $^{64}\text{Cu}$ -labeled nanoparticles needs to be within the detection limits of two modalities for *in vivo* imaging studies. The biodistribution and microPET-CT imaging studies demonstrated a long blood circulation of the probe in BALB/c mice, contributed by the lipid-PEG coating.

Although PET tracers are able to locate the intratumoral areas of uptake with higher spatial resolution, the advantages of combining PET with MRI can provide the possibility of making use of MR images to correct for PET partial-volume effects and to favour PET image reconstruction [34]. Radiolabeled SPIOs conjugated with tumor-specific targeting moieties have been explored as bimodal PET-MR or

SPECT-MR probes for tumor imaging and cancer therapy [35-39]. Polyaspartic acid (PASP)-coated SPIO nanoparticles functionalized with cyclic arginine-glycine-aspartic (RGD) peptides for integrin  $\alpha_v\beta_3$  targeting and DOTA for  $^{64}\text{Cu}$  labeling were developed as dual PET-MR probes of tumor integrin  $\alpha_v\beta_3$  expression (Figure 5) [40]. The SPIO nanoparticles core serving as MR imaging detecting unit were coated with PASP through the carboxyl group; the remaining amine group was used for conjugation with DOTA to radiolabel  $^{64}\text{Cu}$  as PET detecting unit, and to linker NHS-poly(ethylene glycol) (PEG)-maleimide (MAL) for RGD peptides as tumor-targeting unit for integrin  $\alpha_v\beta_3$  positive tumors. *In vivo* PET studies showed that specific binding to tumor reached the highest value ( $10.1 \pm 2.1$  %ID/g) at 4 h after injection of  $^{64}\text{Cu}$ -DOTA-IO-RGD (Figure 6, left). Blocking studies confirmed the specificity toward  $\alpha_v\beta_3$  receptor. *In vivo* MR imaging studies using T2-weighted fast spin-echo on U87MG tumor-bearing mice demonstrated that the signal intensity decreased more after an injection of DOTA-IO-RGD compared with an injection of DOTA-IO and a co-injection of integrin  $\alpha_v\beta_3$ -blocking agent (Figure 6, right).

**Table 2.** Nano-sized bimodal probes and their applications.

Probe	PET(SPECT) reporter	MR reporter	Applications	Ref.
$^{64}\text{Cu}$ -DOTA-ADIO	$^{64}\text{Cu}$	SPIO	Atherosclerotic plaques	32
$^{64}\text{Cu}$ -DOTA-mSPIO	$^{64}\text{Cu}$	SPIO	Disease detection and treatment in atherosclerosis and cancer models	33
$^{64}\text{Cu}$ -NOTA-SPION-cRGD-DOX	$^{64}\text{Cu}$	SPION	U87MG human glioblastoma cell targeting	35
$^{64}\text{Cu}$ -DOTA-USPIO	$^{64}\text{Cu}$	USPIO	Earlier neoplastic lesion detection	36
$^{125}\text{I}$ -cRGD-SSPIO	$^{125}\text{I}$	USPIO	Integrin $\alpha_v\beta_3$ expression in breast cancer	37
$^{111}\text{In}$ -DOTA-di-scFv-NP	$^{111}\text{In}$	SPIO	MUC-1 expression in glandular epithelial cells and AMF therapy	38
$^{111}\text{In}$ -DOTA-ChL6	$^{111}\text{In}$	SPIO	Breast cancer and alternating magnetic field (AMF) therapy	39
$^{64}\text{Cu}$ -DOTA-IO-RGD	$^{64}\text{Cu}$	SPIO	U87MG human glioblastoma cell line, tumor $\alpha_v\beta_3$ integrin expression	40
$^{124}\text{I}$ -SA-MnMEIO	$^{124}\text{I}$	MnFe <sub>2</sub> O <sub>4</sub>	Axillary and brachial lymph nodes (LNs) imaging	41
$^{68}\text{Ga}$ -NOTA-IO-Man	$^{68}\text{Ga}$	SPIO	LNs imaging	42
$^{111}\text{In}$ -mAbMB-SPION	$^{111}\text{In}$	SPION	Mesothelioma imaging	43
$^{64}\text{Cu}$ -dtcbp-SPION	$^{64}\text{Cu}$	SPION	LNs mapping	44
$^{64}\text{Cu}$ -dtcbp-MnFe <sub>2</sub> O <sub>4</sub> and $^{18}\text{F}$ -MnFe <sub>2</sub> O <sub>4</sub>	$^{64}\text{Cu}$ and $^{18}\text{F}$	MnFe <sub>2</sub> O <sub>4</sub>	Targeted organs (liver, spleen)	45
$^{99\text{m}}\text{Tc}$ -SPIONs	$^{99\text{m}}\text{Tc}$	SPION	SLN mapping	46
$^{68}\text{Ga}$ -NODA-Magh-1-PNPs	$^{68}\text{Ga}$	SPIO	PET-MR diagnostic probe	47
$^{99\text{m}}\text{Tc}$ -USPIO	$^{99\text{m}}\text{Tc}$	USPIO	MPS theranostic probe	48, 49
$^{68}\text{Ga}$ -DTPA-USPIO	$^{68}\text{Ga}$	USPIO	MPS theranostic probe	50
$^{99\text{m}}\text{Tc}$ -DPA-ale Endorem	$^{99\text{m}}\text{Tc}$	SPION	MPS system imaging	51
$^{99\text{m}}\text{Tc}$ -PEG(5)-BP-USPIO	$^{99\text{m}}\text{Tc}$	USPIO	Cardiovascular imaging	52
$^{99\text{m}}\text{Tc}$ -DTPA-SPION-LBA	$^{99\text{m}}\text{Tc}$	SPION	Hepatocyte imaging	54
$^{64}\text{Cu}$ -DOTA-MDIO	$^{64}\text{Cu}$	SPIO	Macrophage-targeting atherosclerotic plaque imaging	55
$^{64}\text{Cu}$ -DOTA-IO	$^{64}\text{Cu}$	SPIO	Vascular inflammation mapping	56
$^{68}\text{Ga}$ -NOTA-IO-IONP	$^{68}\text{Ga}$	SPIO	HT-29 colon cancer cells targeting	57
$^{68}\text{Ga}$ -DOTA-IO-GUL	$^{68}\text{Ga}$	SPIO	Prostate-specific membrane antigen (PSMA)	58
$^{99\text{m}}\text{Tc}$ -USPIO-C595	$^{99\text{m}}\text{Tc}$	USPIO	Breast cancer and MPS	59
$^{11}\text{C}$ -SPION	$^{11}\text{C}$	SPION	Liver imaging	60
Fe <sub>3</sub> O <sub>4</sub> -Ag <sup>125</sup> I heterodimer	$^{125}\text{I}$	SPIO	MPS uptake	61
$^{89}\text{Zr}$ -DFO-ferumoxytol	$^{89}\text{Zr}$	SPIO	Prostate cancer and LNs diagnosis	62
$^{64}\text{Cu}$ -SPION	$^{64}\text{Cu}$	SPION	Chelator-free radiolabeling	65
$^{89}\text{Zr}$ -FH	$^{89}\text{Zr}$	Feraheme	Chelator-free radiolabeling	66
$^{68}\text{Ga}$ -SPION	$^{68}\text{Ga}$	SPION	Chelator-free radiolabeling	71
As <sup>3+</sup> As <sup>5+</sup> SPION	As <sup>3+</sup> As <sup>5+</sup>	SPION	Chelator-free radiolabeling	72
$^{57}\text{Co}$ -SPION	$^{57}\text{Co}$	SPION	Chelator-free radiolabeling	73
$^{69}\text{Ge}$ -SPION	$^{69}\text{Ge}$	SPION	SLN	74

<sup>99m</sup> Tc-BP-S-MWNT	<sup>99m</sup> Tc	SPION	In carbon nanotubes for MPS uptake	83, 84
<sup>68</sup> Ga-AGuIX-DOTA-Gd	<sup>68</sup> Ga	Gd-DOTA	Intravenous injection for biodistribution	85
Gd(DOTA) <sup>111</sup> In(DOTA)SRPs	<sup>111</sup> In	Gd-DOTA	Intravenous injection for biodistribution	87
GdAcAc-DTPA- <sup>166</sup> Ho and GdAcAc-DTPA- <sup>99m</sup> Tc	<sup>166</sup> Ho and <sup>99m</sup> Tc	GdAcAc	In liposome for diagnosis and therapy	90
<sup>89</sup> Zr-Gd-DTPA-OL	<sup>89</sup> Zr	Gd-DTPA	In liposome for imaging of cancer	91
<sup>64</sup> Cu-EP-2104R	<sup>64</sup> Cu	Gd-DOTA	Fibrin-targeted thrombus imaging	93, 94
<sup>99m</sup> Tc-Bis-pyridyl-lysine-caproyl-phosphatidyle thanolamine-Gd-DTPA	<sup>99m</sup> Tc	Gd-DTPA	α <sub>v</sub> β <sub>3</sub> integrin targeted Vx2 rabbit tumor	95

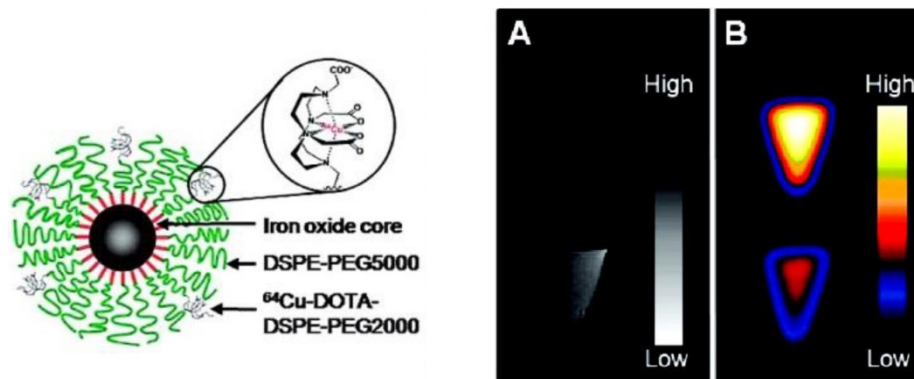


**Figure 4.** (Left) Schematic representation of dual-modality <sup>64</sup>Cu-mSPIO. (Right) PET and MR imaging of <sup>64</sup>Cu-mSPIO phantoms. (A) T<sub>2</sub>-weighted image of 25 μg Fe/mL (bottom) of <sup>64</sup>Cu-labeled magnetic nanoparticles (scale bar corresponds to high and low iron concentration). (B) Decay-corrected microPET image of 25 μg Fe/mL (top) and 10 μg Fe/mL (bottom) of <sup>64</sup>Cu-labeled magnetic nanoparticles (scale bar corresponds to high and low copper-64 concentration). Adapted with permission from [33], copyright 2010 American Chemical Society.

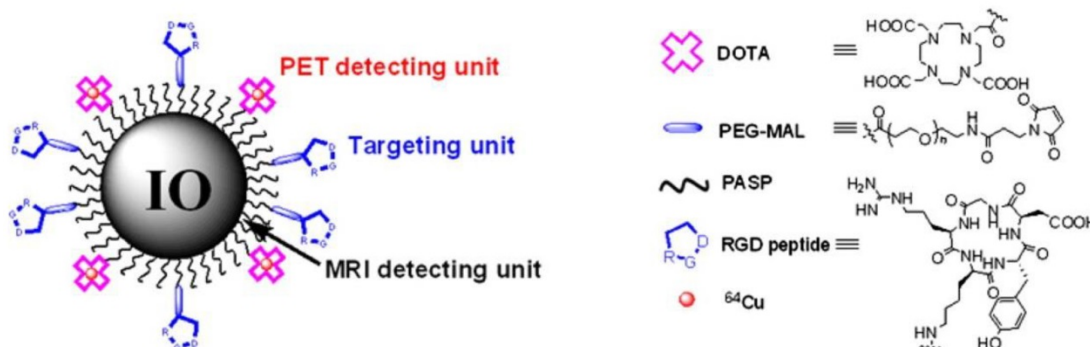


**Figure 5.** Illustration of PET-MRI probe based on IO nanoparticles. Adapted with permission from [40], copyright 2008 Society of Nuclear Medicine and Molecular Imaging.

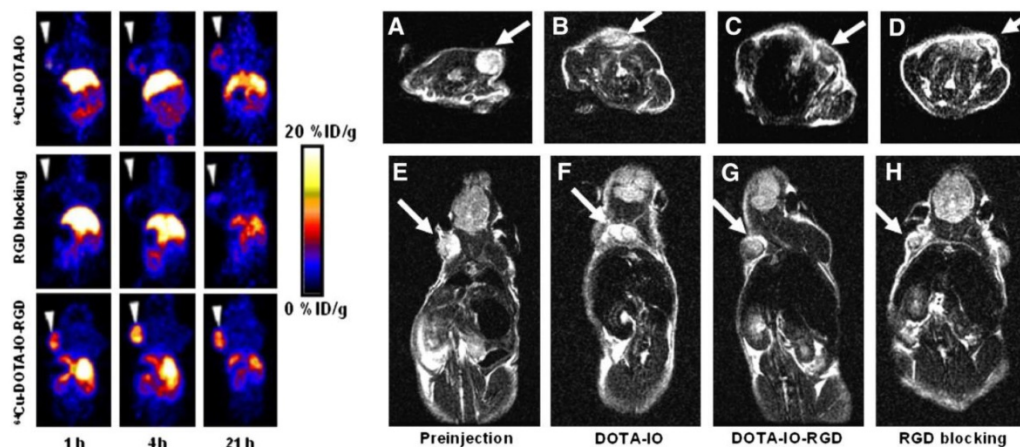


**Figure 6.** (Left) Decay-corrected whole-body coronal PET images of nude mice bearing human U87MG tumor at 1, 4, and 21 h after injection of 3.7 MBq of <sup>64</sup>Cu-DOTA-IO, <sup>64</sup>Cu-DOTA-IO-RGD, or <sup>64</sup>Cu-DOTA-IO-RGD with 10 mg of c(RGDyK) peptide per kg (300 μg of iron-equivalent IO particles per mouse). (Right) T<sub>2</sub>-weighted MR images of nude mice bearing U87MG tumor before injection of IO nanoparticles (A and E) and at 4 h after tail-vein injection of DOTA-IO (B and F), DOTA-IO-RGD (C and G), and DOTA-IO-RGD with blocking dose of c(RGDyK) (D and H). Adapted with permission from [40], copyright 2008 Society of Nuclear Medicine and Molecular Imaging

Radiolabeled SPIOs as bimodal probes have potential clinical applications in the preoperative localization and characterization of sentinel lymph nodes (SLNs), which could provide information of their pathology for investigation of tumor metastasis. SPIOs with a composition of  $\text{MnFe}_2\text{O}_4$  (MnMEIO) coated with serum albumin (SA) were used to radiolabel the protein with  $^{124}\text{I}$  ( $^{124}\text{I}$ -SA-MnMEIO) as a bimodal imaging probe to image SLNs *in vivo* [41].  $^{124}\text{I}$ -SA-MnMEIO can be directly radiolabeled by conjugation of radionuclide  $^{124}\text{I}$  to the ortho position of tyrosine residue in SA through using Iodo-Beads.  $^{124}\text{I}$  ion from Iodo-Beads in solution will be oxidized to form a reactive  $^{124}\text{I}^+$ , which reacts with the ortho position of tyrosine. Two different LNs, brachial and axillary LNs, could be clearly identified and localized in PET-MR fusion image; though, axillary LN was unambiguously spotted when MRI single modality was used only due to its location far from the injection site compared with brachial LN (Figure 7). Since SLNs are located deep inside tissue, it is quite challenge to image SLNs. This example demonstrated the advantages of using a PET-MR bimodal probe to image SLNs, which can be used to further evaluate the metastatic status of a tumor.

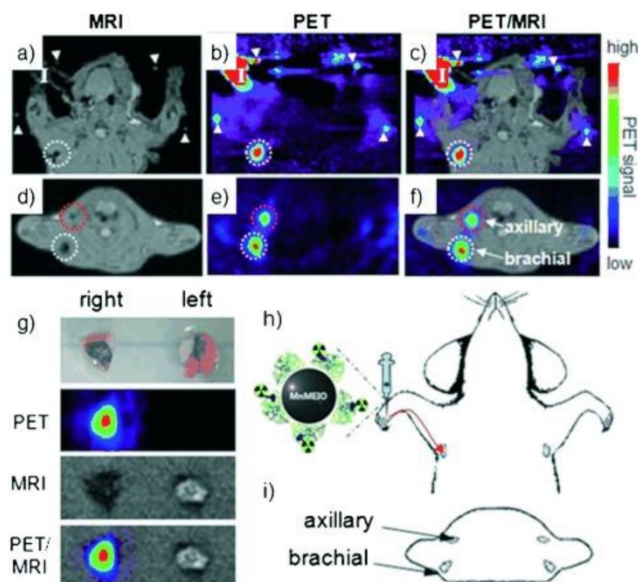


**Figure 7.** (a–f) PET-MR images of SLNs in a rat at 1 h post injection of  $^{124}\text{I}$ -SA-MnMEIO into the right forepaw (I = nanoprobe injection site). Coronal a) MR and b) PET images in which a brachial LN (white circle) is detected. c) The position of the brachial LN is well matched in a PET-MR fusion image. Four small pipette tips containing  $\text{Na}^{124}\text{I}$  solution were used as a fiducial marker (white arrowheads) for the concordant alignment in PET-MR images. In the transverse images, axillary (red circle) and brachial LNs (white circle) are detected in the d) MR and e) PET images, and images of each node are nicely overlapped in the corresponding PET/MR fusion image (f). g) The explanted brachial LN also shows consistent results with *in vivo* images by PET and MR. Only the LN from the right-hand side of the rat containing  $^{124}\text{I}$ -SA-MnMEIO shows strong PET and dark MR images. The schematics of the rat in the h) coronal and i) transverse directions show the locations of the LNs. Adapted with permission from [41], copyright 2008 Wiley-VCH.

A dual PET-MR imaging probe  $^{68}\text{Ga}$ -NOTA-IO-MAN was synthesized by a new methodology for targeting LNs [42]. SPIOs were encapsulated in a solution of polysorbate 60 with functionalized amphiphiles—NOTA conjugated with stearylamine (NOTA-SA) and  $\alpha$ -D-mannopyranosylphenyl isothiocyanate conjugated with stearylamine (Man-SA); the resulting monodisperse and stable SPIOs were radiolabeled with  $^{68}\text{Ga}$  for PET-MR imaging of LNs. When  $^{111}\text{In}$ -labeled anti-mesothelin antibody (mAbMB) was conjugated to the SPIO nanoparticles, a dual-modal imaging probe was developed for SPECT-MR imaging of mesothelin-expressing cancers [43]. The bimodal imaging provided functional and anatomical information for early diagnosis and treatment planning of these cancers.

A different strategy was developed to radiolabel clinically approved SPIOs such as Endorem/Feridex. A bifunctional chelator dithiocarbamate bisphosphonates (DTCBP) was conjugated with Endorem with high affinity for both the metallic radionuclide  $^{64}\text{Cu}$  and dextran-coated SPIO nanoparticles to facilitate the radiolabeling in high yields, providing a highly stable bimodal probe both *in vitro* and *in vivo* (Figure 8, left) [44]. However, the disadvantage of this probe is that radiolabeling of  $^{64}\text{Cu}$  to the DTCBP needs to be done before conjugation with Endorem, resulting in low specific activity of the tracer. Preclinical PET-MR imaging studies of C57BL/6 mice demonstrated that the MR signal decreased significantly in the popliteal LNs (Figure 8, right (B)), PET-CT images showed uptake of  $^{64}\text{Cu}(\text{DTCBP})_2$ -Endorem in the popliteal LNs and less uptake in the iliac LNs (Figure 8, right (C) and (D)). No translocation of  $^{64}\text{Cu}(\text{DTCBP})_2$ -Endorem was found. PET-MR imaging studies confirmed the dual probe's potential for imaging SLN in a non-tumor model. A similar strategy used an aluminium hydroxide coating to stabilize the magnetic nanoparticles  $\text{Fe}_3\text{O}_4$  and  $\text{MnFe}_2\text{O}_4$  for conjugation with radiolabeled  $^{64}\text{Cu}(\text{DTCBP})_2$  as dual modality PET-MR probes [45]. SPIOs radiolabeled with  $^{99\text{m}}\text{Tc}$  were reported as a dual SPECT-MR probe feasible for imaging SLNs [46]. Both SPECT and MR images showed the accumulation of  $^{99\text{m}}\text{Tc}$ -SPIOs in LNs after subcutaneous injection in rats. The high uptake of  $^{99\text{m}}\text{Tc}$ -SPIOs found in SLN from biodistribution studies indicated  $^{99\text{m}}\text{Tc}$ -SPIOs could have future applications in breast cancer and malignant melanoma.

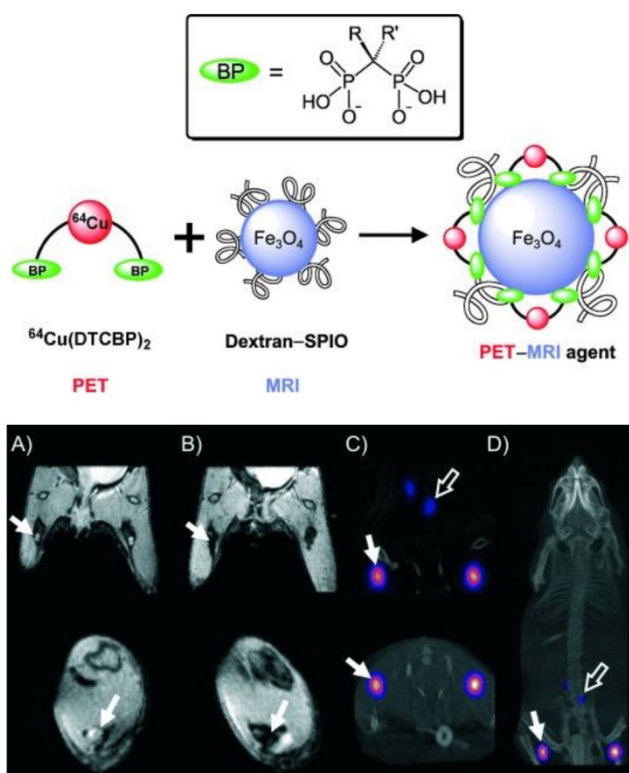


**Figure 8.** (Top) Radiolabeling of dextran-coated iron oxide nanoparticles such as Endorem using radiolabeled bisphosphonates (BPs). (Bottom) In vivo PET-MR imaging studies with [<sup>64</sup>Cu(dtcbp)<sub>2</sub>]-Endorem in a mouse. (A, B) Coronal (top) and short axis (bottom) MR images of the lower abdominal area and upper hind legs showing the popliteal lymph nodes (solid arrows) before (A) and after (B) footpad injection of [<sup>64</sup>Cu(dtcbp)<sub>2</sub>]-Endorem. (C) Coronal (top) and short-axis (bottom) NanoPET-CT images of the same mouse as in (B) showing the uptake of [<sup>64</sup>Cu(dtcbp)<sub>2</sub>]-Endorem in the popliteal (solid arrow) and iliac lymph nodes (hollow arrow). (D) Whole-body NanoPET-CT images showing sole uptake of [<sup>64</sup>Cu(dtcbp)<sub>2</sub>]-Endorem in the popliteal and iliac lymph nodes. No translocation of radioactivity to other tissues was detected. Adapted with permission from [44], copyright 2011 Wiley-VCH.

The nanoparticle size and coating of radiolabeled SPIOs are crucial for the dual modal probe's biodistribution, which can affect the excretion pattern of the probe. Maghemite nanoparticles were encapsulated in poly(D,L-lactide-co-glycolide)-block-poly(ethylene glycol) copolymer (PLGA-b-PEG-COOH), resulting in better biocompatibility for hybrid imaging [47]. The biodistribution of <sup>99m</sup>Tc- or <sup>67</sup>Ga-radiolabeled ultra SPIO nanoparticles in Balb/c mice showed high uptake in reticuloendothelial organs such as spleen and liver [48-50]. The <sup>99m</sup>Tc-radiolabeled bisphosphonate (BP), <sup>99m</sup>Tc-dipicolylamine-alendronate (<sup>99m</sup>Tc-DPA-ale), can be directly conjugated to the surface of uncoated SPIO nanoparticles, as was firstly reported for a SPECT-MR dual-modal probe [51]. <sup>99m</sup>Tc-DPA-ale binds to the core of Endorem, where it does not affect the dextran coating of the nanoparticles. This provided a synthetic methodology for the BP group to attach functional groups to the SPIO nanoparticles. However, a short circulation time was found in the

biodistribution studies because the radiolabeled nanoparticles were quickly taken up by macrophages of the mononuclear phagocyte system (MPS). A new type of ultra-small SPIO with a coating based on a bisphosphonate-anchored PEGylation (PEG(5)-BP-USPIO) was developed to prevent uptake by MPS and resulted in extended circulation times (Figure 9) [52,53]. The stable hydrophilic PEGylation coating led to colloidal stability of PEG(5)-BP-USPIO. PEG(5)-BP-USPIOs demonstrated high r<sub>1</sub> and low r<sub>2</sub> relaxivities, making it an effective T1-weighted contrast agent. Considerable signal increase from *in vivo* MRI studies indicated its high potential for MR angiography. *In vivo* SPECT studies confirmed its long blood circulation time and revealed its decomposition and excretion patterns. Through synthetic design and chemical modifications, the radiolabeled SPIO nanoparticles can be developed as targeted hybrid imaging probes, such as for hepatocytes targeting by surface modification with lactobionic acid [54], macrophages targeting via scavenger receptor type A by modification with maleic anhydride to increase the negative charge [55, 56], and HT-29 cancer cells [57], prostate-specific membrane antigen [58] and MUC-1-positive breast cancer cells targeting [59] by conjugation with oleonic acid, glutamate-urea-lysine and monoclonal antibody C595 mAb, respectively. However, their *in vivo* targeting ability would be affected due to coverage of the targeting sites by protein corona [59].

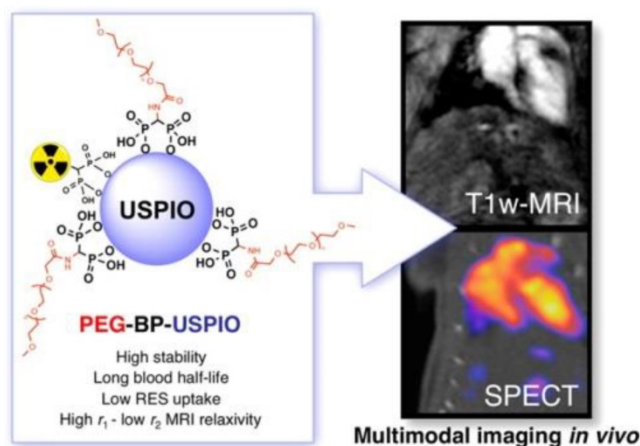


**Figure 9.** Long-circulating bimodal nanoparticles for PET-MR and SPECT-MRI. (A) Bisphosphonate anchors allow strong and stable binding of PEG polymers and radionuclides on the surface of the USPIOs. (B) The bimodal nanoparticles circulate in the bloodstream, as indicated by the strong imaging signal in the heart and vessels. Adapted with permission from [52], copyright 2013 American Chemical Society.

New synthetic strategies for preparing SPIO nanoparticle-based bimodal PET-MR and SPECT-MR probes are emerging. Carbon-11 radiolabeled SPIOs are one example [60]. Similar to routine radiolabelling

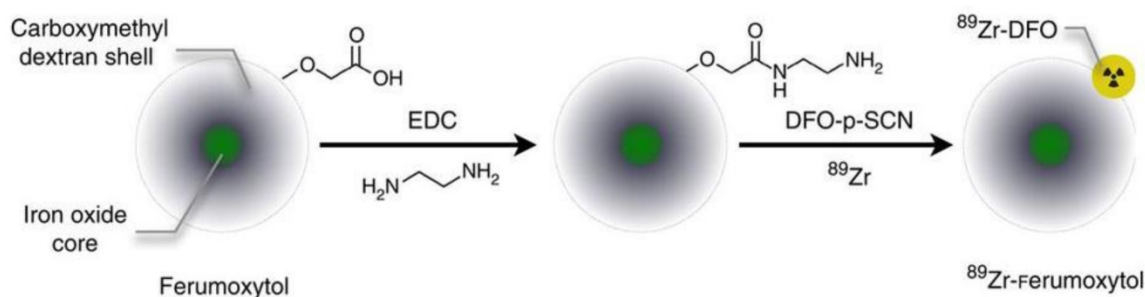


**Figure 10.** Schematic of the carboxyl-terminated polyglucose sorbitol carboxymethylether coating (grey) surrounding the iron oxide crystal core (green) of the nanoparticle. Amination of the particles was carried out before their functionalization with ~7 DFO chelates. Adapted with permission from [62], copyright 2014 Springer Nature.

of small molecular carbon-11-containing PET tracers, carbon-11 from the [ $^{11}\text{C}$ ]methyl iodide reacts with carboxylic acid ( $-\text{COOH}$ ) and amine ( $-\text{NH}_2$ ) functional groups at the surface of SPIO nanoparticles via N- and O-methylation. Due to nanoparticle agglomeration, the proof-of-concept methodology needs to be improved to increase radiochemical yield before the bimodal probe can be applied to *in vivo* studies. Novel dual-modality probes,  $^{125}\text{I}$ -radiolabel  $\text{Fe}_3\text{O}_4\text{-Ag}^{125}\text{I}$  heterodimer nanoparticles, were synthesized through direct reaction of sodium iodine-125 with  $\text{Fe}_3\text{O}_4\text{-Ag}$  hetero-structured nanoparticles [61]. Radiolabeling of  $^{89}\text{Zr}$  to the organic coating of SPIOs was reported as a bimodal probe to image SLN [62]. The carbohydrate-coated SPIO nanoparticle Ferumoxytol, an FDA-approved drug for MRI contrast and the treatment of iron deficiency anemia, was conjugated to desferrioxamine (DFO) chelate to generate the PET-MR dual modal probe  $^{89}\text{Zr}$ -DFO-labeled ferumoxytol ( $^{89}\text{Zr}$ -ferumoxytol) for mapping deep-tissue LNs (Figure 10). As a synthetic strategy,  $^{89}\text{Zr}$ -DFO has been employed to conjugate the albumin colloid covalently for preclinical drainage mapping of LNs in rabbit [63] and man [64], respectively. The conjugation did not significantly affect the physicochemical properties and consequent relaxivities of the nanoparticles. PET-MR studies showed that  $^{89}\text{Zr}$ -ferumoxytol can not only localize the drainage to the brachial and axillary LN in healthy mice but also can map the draining lymphatics in the disease mouse model [62].

Chelator-free approaches and core-doping for radiolabeling nanoparticles have been used for development of PET/SPECT-MR bimodal probes. Radiometals can be attached to the nanoparticle surface or incorporated into the particle core. The synthesis of dextran-coated  $^{64}\text{Cu}$ -doped iron oxide nanoparticles was reported as the first example of core-doped  $^{64}\text{Cu}$  particles. The  $^{64}\text{Cu}$  radionuclide was added to the reaction mixture before nanoparticle synthesis so that the radionuclide could be incorporated straightforwardly into the nanoparticle

core during subsequent standard synthesis of the dextran-coated USPIOs [65]. Microwave heating-induced chelator-free  $^{64}\text{Cu}$  doping of USPIOs was elegantly demonstrated. A similar heat-induced method was employed to synthesize chelator-free radiolabeled  $^{89}\text{Zr}$ -Feraheme (FH) nanoparticles (Figure 11) [66]. This experimental approach can be applicable to other radiometals such as  $^{64}\text{Cu}$  and  $^{111}\text{In}$  with different oxidation states. The *in vitro* ligand exchange and plasma stability studies showed  $^{89}\text{Zr}$ -FH was thermodynamically and kinetically stable. PET-CT imaging and biodistribution studies showed that the physical and biological properties of the FH nanoparticles were not affected by  $^{89}\text{Zr}$  radiolabeling. More recently, heat-induced radiolabeling nanoparticles with radiometal were reported as multimodal and multifunctional probes, by a mature synthetic protocol [67], by using click chemistry to attach alkyne azide as a linker to conjugate with bioactive group [68], for promising applications such as monocyte tracking [69] and characterization of mature B cell accelerating wound healing [70]. A microwave-driven protocol was used for fast synthesis of  $^{68}\text{Ga}$ -radiolabeled SPIONs as the first example of  $^{68}\text{Ga}$  core-doped nanoparticles for PET-MR imaging [71]. Chelator-free radiolabeling, was developed as a highly efficient strategy for synthesis of arsenic $^{3+}$  and arsenic $^{5+}$  ions-radiolabeled SPIONs as PET-MR probes. Both  $\text{As}^{3+}$  and  $\text{As}^{5+}$  radiometal ions display high affinity and specific chemical reactivity with the surface of SPIONs through radiolabeling reaction [72]. Chelator-free radiolabeling was applied to incorporate radiometal ions such as  $^{57}\text{Co}$ ,  $^{67}\text{Ga}$ ,  $^{64}\text{Cu}$  into SPIONs to provide PET/SPECT-MR probes. The radiochemical yields depended on reaction conditions such as temperature, pH and reaction time, which were investigated and optimized. The  $^{57}\text{Co}$ ,  $^{67}\text{Ga}$ ,  $^{64}\text{Cu}$ -radiolabeled SPIONs were sterically stable. No dissociated radionuclides from the nanoparticles in various physiological media were detected [73].

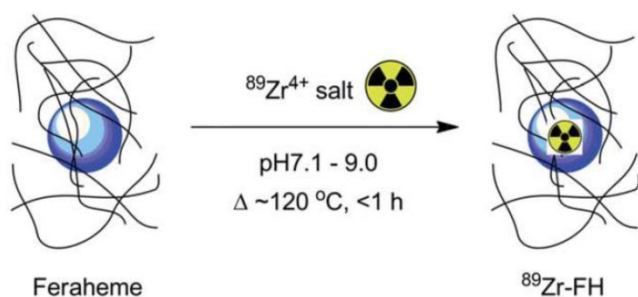


**Figure 11.** Reaction of FH with  $^{89}\text{Zr}^{4+}$  ion salts (oxalate or chloride) to give radiolabeled  $^{89}\text{Zr}$ -FH. Adapted with permission from [66], copyright 2015 Royal Society of Chemistry.

Inspired by the technology that the parent  $^{68}\text{Ge}$  radionuclide in the  $^{68}\text{Ge}/^{68}\text{Ga}$  generator is bound to metal oxide  $\text{TiO}_2$ , the SPIONs were labeled with  $^{89}\text{Ge}$  in the absence of a chelator as a PET-MR probe. By incorporating PET radionuclides such as  $^{69}\text{Ge}$  and  $^{59}\text{Fe}$  into SPIOs without a chelator during the nanoparticle synthesis is one of the new synthetic approaches to generating multimodal nanoparticles. For example, a dual PET-MR probe  $^{69}\text{Ge}$ -SPION@PEG was prepared by incorporating  $^{69}\text{Ge}$ , which was generated by  $^{69}\text{Ga}(p,n)^{69}\text{Ge}$  from a cyclotron, into SPIOs for imaging SLN. The hydrophilic coating poly(acrylic acid) (PAA) of SPION was PEGylated to increase the *in vivo* stability (Figure 12, left). Uptake of  $^{69}\text{Ge}$ -SPION@PEG in normal BALB/c mice in the popliteal LN from *in vivo* PET images and contrast enhancement in MR images demonstrated its application in LN mapping [74] (Figure 12, right). Different preparation methods to incorporate  $^{59}\text{Fe}$  into SPIOs were reported [75]. An efficient post-synthesis radiolabeling of monodisperse SPIOs, which were derived from high thermal decomposition of precursor and stabilized by oleic acid, was achieved through incubation with  $^{56}\text{Fe}$ . Core labeling of  $^{56}\text{Fe}$  can overcome the issue of probe stability *in vivo*, in which the radiolabelling moiety

would decompose from the nanostructure.  $^{14}\text{C}$ -oleic acid was used to stabilize the SPIOs during the synthesis. Only a small amount of oleic acid was replaced by the polymer during encapsulation. *In vivo* studies of  $^{59}\text{Fe}$ -SPIOs provided a precise biological profile. However, direct incorporation of radionuclide into SPIOs was potentially only used in preclinical studies such as biodistribution, specific targeting, and metabolism of functional nanoparticles.

Carbon nanotubes (CNTs) have been used as promising nanomaterials in biomedicine [76]; they have been proposed as a useful nanoplatform for PET/SPECT-MR imaging probes. One of the synthetic strategies for preparing CNTs-based imaging probes is to form hybrid nanostructures either by filling the cavity with imaging reporters or by external attachment of imaging reporters. For example, PET/SPECT radionuclides-labeled chelates were conjugated to the external CNT walls for both diagnosis and therapeutics [77-79].  $\text{Gd}^{3+}$  was loaded to CNTs [80] and SPION was attached to CNTs [81] as positive and negative CAs, respectively. Conjugation of SPION to multi-walled CNTs (MWNTs) through electrostatic interactions could be used for diagnosis of liver metastases [82]. CNTs were further used as a nanoplatform for carrying dual SPECT-MR probes. The SPIO nanoparticles were attached to one end of the nanotubes. The resulting SPION-decorated MWNTs were radiolabeled with  $^{99\text{m}}\text{Tc}$  through a functionalized bisphosphonate (dipicolylamine-alendronate, DPAAle) on the carbon nanotube surface as opposed to non-selective adsorption of the radioisotope to the MWNTs [83] (Figure 13). *In vivo* biodistribution and MR imaging studies showed remarkable MR signal enhancement for the shortened hybrid CNTs compared to their longer hybrid counterparts [84].

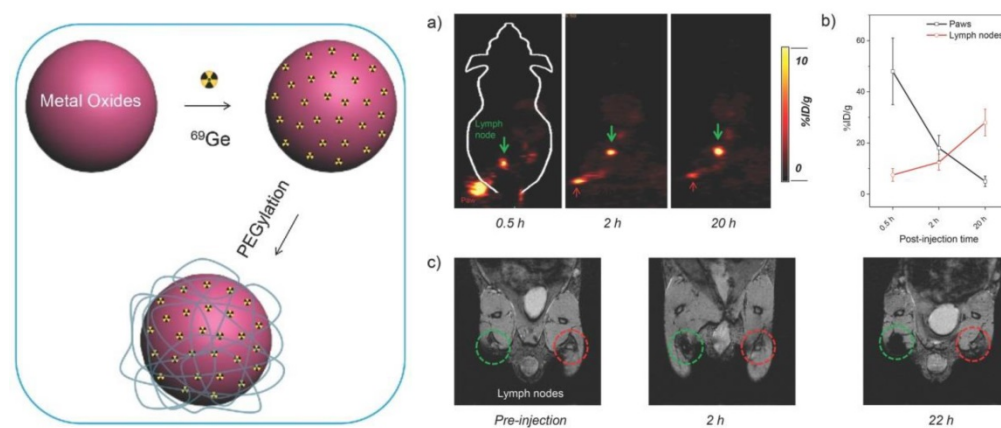


**Figure 12.** (Left) A schematic illustration of chelator-free synthesis of  $^{69}\text{Ge}$ -metal oxides. (Right) a) *In vivo* lymph node imaging with PET after subcutaneous injection of  $^{69}\text{Ge}$ -SPION@PEG into the left footpad of the mouse. Lymph nodes and paws are indicated by green and red arrows, respectively. b) Quantification of the  $^{69}\text{Ge}$ -SPION@PEG uptake in the lymph node and mouse paw ( $n = 3$ ). c) *In vivo* lymph node mapping with MRI before and after injection of Ge-SPION@PEG into the left foot pad of the mouse. Obvious darkening of the lymph node can be seen (dashed green circle), whereas no contrast enhancement is observed for the contralateral lymph node (dashed red circle). Adapted with permission from [74], copyright 2014 Wiley-VCH.

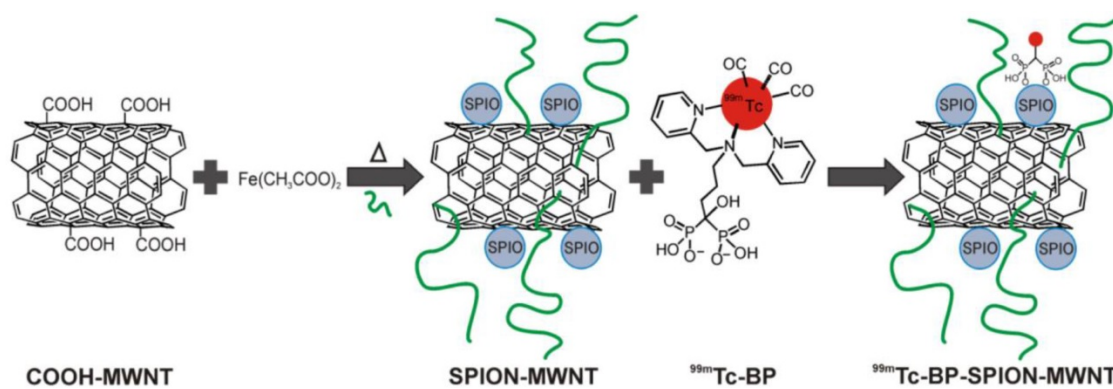


**Figure 13.** Radio-labelling of SPION-MWNT hybrids with technetium-99m ( $^{99m}\text{Tc}$ ) via a linker. The Radio-labelling was conducted using  $^{99m}\text{Tc}$ -dipicolylamine-alendronate ( $^{99m}\text{Tc}$ -DPAale). Adapted with permission from [83], copyright 2014Wiley-VCH.

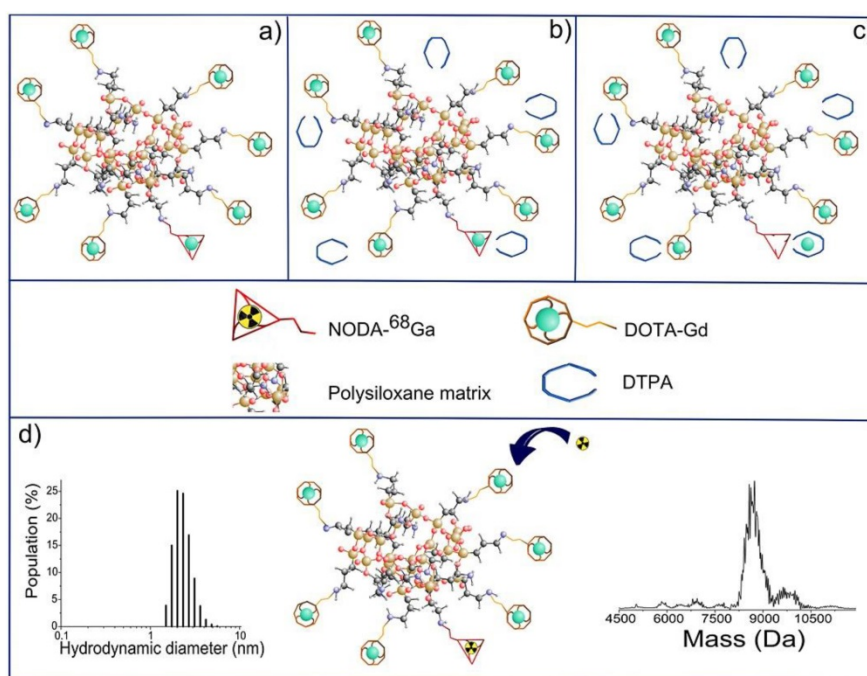


**Figure 14.** Final steps in the synthesis of AGuIX nanoparticles: (a) nanoparticles after transfer in water; (b) addition of DTPA ligands; (c) chelation of  $\text{Gd}^{3+}$  previously trapped in NODAGA ligands; (d) possibility of radiolabelling with  $^{68}\text{Ga}$  on accessible NODAGA ligands. On the left is the dynamic light scattering distribution of AGuIX and on the right is their mass distribution determined by deconvolution with a multiplicative correlation algorithm. Adapted with permission from [85], copyright 2011Wiley-VCH.

Small and rigid platforms (SRPs) of polysiloxane matrix-based  $\text{Gd}_2\text{O}_3$  core- $\text{SiO}_x$  shell particles (AGuIX) were reported to incorporate the chelators DOTAGA (1,4,7,10-tetraazacyclododecane-1-glutaric anhydride-4,7,10-triacetic acid) and NODAGA (2,2'-(7-(1-carboxy-4-((2,5-dioxopyrrolidin-1-yl)oxy)-4-oxobutyl)-1,4,7-triazonane-1,4-diyl)diacetic acid), for  $\text{Gd}^{3+}$  coordination as MR imaging reporter and for  $\text{Ga}^{3+}$  radiolabelling as PET reporter, respectively [85]. *In vivo* MR imaging showed that the high r1 relaxivity of the bimodal nanoparticles led to signal enhancement in the kidneys. The extremely small and monodisperse nanoparticles with several Gd and  $^{68}\text{Ga}$  ions on their surface could be cleared by renal excretion. Signal co-localization from PET and MR

imaging confirmed the nanoparticle elimination pattern. The top-down synthetic approach was used for preparing bimodal nanoparticles [86]. Firstly, the gadolinium oxide  $\text{Gd}_2\text{O}_3$  core was synthesized and coated with a polysiloxane shell. Then, the resulting  $\text{Gd}_2\text{O}_3$ - $\text{SiO}_x$  core-shell particles were encapsulated with DOTAGA chelator. Finally, free  $\text{Gd}^{3+}$  dissociated from the  $\text{Gd}_2\text{O}_3$  core chelate to DOTAGA. The dissolution of the core resulted in fragmentation of the nanoparticles into SRPs of polysiloxane. DTPA was introduced via transmetalation of  $\text{Gd}^{3+}$  from NODAGA, which would offer radiolabelling (Figure 14). The nanoparticle composition was fully characterized. The rigid structure of SRPs led to substantial contrast enhancement for MR. These SRPs

can be further conjugated with Cy5.5 fluorophores as trimodal probes for MR, PET/SPECT, and fluorescence imaging [87].

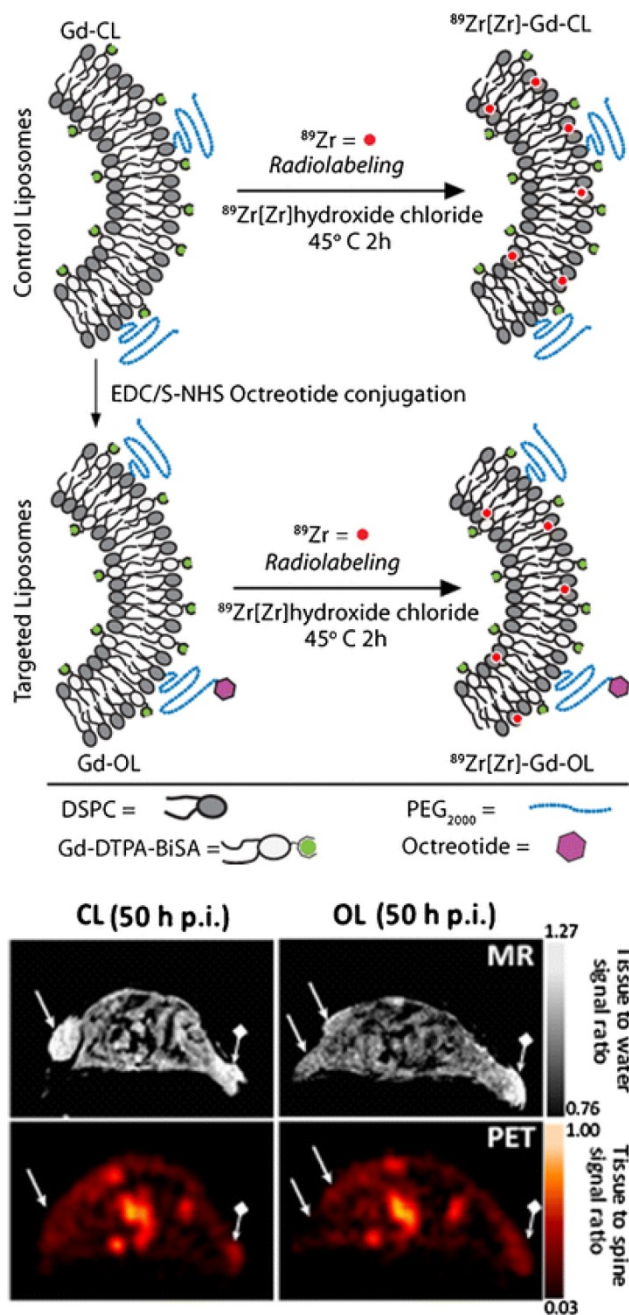


**Figure 15.** (Top) LP constructs and radiolabeling strategy: OCT was conjugated to Gd-Control LPs (CL) resulting in targeted OCT-LP (OL). Both paramagnetic formulations were radiolabeled using  $^{89}\text{Zr}$  with a chelator-free approach. (Bottom) PET-MR co-registration: MR (top row) and PET (bottom) scans of mice bearing wild type (wt) ( $\rightarrow$ ) and SSTR2-positive tumors ( $\blacklozenge\rightarrow$ ) and injected with CL (left panel) and OL (right panel). Adapted with permission from [91], copyright 2013 Springer Nature.

Liposomes (LPs) have been used as a carrier system to deliver tumor-targeting antibody or peptide for cancer treatment or therapy [88, 89]. By incorporating paramagnetic gadolinium and then labeling with radionuclides such as  $^{166}\text{Ho}$  or  $^{99\text{m}}\text{Tc}$ ,

liposomes can be used as bimodal SPECT-MR imaging probes. Nano-sized LPs co-loaded with gadolinium-acetylacetonate (GdAcAc) and radiolabeled with  $^{166}\text{Ho-DTPA}$  (GdAcAc-DTPA-Ho) proved to be a very promising multimodal imaging probe for therapy applications [90]. Novel  $^{89}\text{Zr}$ -radiolabeled paramagnetic LPs conjugated with octreotide were developed as PET-MR probes for imaging somatostatin receptor subtype 2 (SSTR2) targeting neuroendocrine tumors [91]. Long-circulating PEGylated LP was used for evaluation of *in vitro* and *in vivo* specific SSTR2 recognition through OCT conjugation. Direct  $^{89}\text{Zr}$ -radiolabeling without chelator was achieved (Figure 15). Tracking of a long-circulating dual PET-MR probe was demonstrated. At 50 h post-injection, co-registered PET-MR imaging showed clear tumor identification. SSTR2 tumor-specific contrast by octreotide-liposome (OL) was highlighted compared to control-liposome (CL).

EP-2104R is a fibrin-targeting Gd-based MR CA in which a six amino-acid cyclic peptide is conjugated to four Gd(DOTA) chelates [92]. EP-2104R was partially depleted of  $\text{Gd}^{3+}$  by DTPA ligand and then chelated with  $^{64}\text{Cu}$  to make a fibrin-targeting dual PET-MR probe for simultaneous PET and MR imaging of thrombus [93]. The thrombus in a rat arterial thrombus model was clearly identified with both PET and MR images [94]. Lipophilic Gd(DTPA) was incorporated into the outer phospholipid layer of the integrin  $\alpha_v\beta_3$ -targeted  $^{99\text{m}}\text{Tc}$  nanoparticles to make a SPECT-MR imaging probe for tumor angiogenesis with 3D neovascular mapping [95]. *In vivo* studies showed that initial treatment of  $\alpha_v\beta_3$ -targeted  $^{99\text{m}}\text{Tc}$ -gadolinium nanoparticles weakens MR contrast enhancement in neovascular imaging. Tumor angiogenesis was characterized by  $\alpha_v\beta_3$ -targeted paramagnetic nanoparticles with MR functionality and  $^{99\text{m}}\text{Tc}$  labelling in a Vx2 model for SPECT-CT acquisition.

### Small molecular trimodal probes

Trimodal imaging has emerged as a novel imaging strategy for translational research, which combines three different modalities together such as PET/SPECT-MR-Optical to provide complementary information and achieve synergistic advantages over any single modality alone. The main challenge of trimodal imaging lies in developing an efficient platform that incorporates various imaging modality reporters without disturbing each other while maintaining the entity intact. Photoacoustic tomography (PAT) provides high-resolution functional and molecular optical imaging with remarkably increased imaging depth by using the

photoacoustic effect of light absorbers compared with traditional optical imaging [96]. Nanoparticles and melanin have been used as exogenous and intrinsic contrast agents for functional and molecular PAT, respectively.

A single small molecule is unlikely to be designed as a trimodal imaging probe due to its limited loading capacity. Only one example of a proposed trimodal PET-MR-fluorescence imaging probe in a single small molecule has been reported (Figure 16) [97]. Gd(DO3A-AM)-Cu(porphyrin) is comprised of Gd<sup>3+</sup>-chelated tetraazacycloalkane Gd(DO3A-AM) as MRI CA, a free-base porphyrin for <sup>64</sup>Cu complex Cu(porphyrin) as a PET tracer and porphyrin macrocycles as fluorescence reporters. The molecules in which paramagnetic metallo-porphyrins were coordinated with Gd as MRI CA and radiolabeled with <sup>99m</sup>Tc and <sup>111</sup>In porphyrins as SPECT tracer were reported as bimodal imaging

probes for tumor imaging due to their preferential tumor uptake [98, 99]. The water-soluble hetero-bimetallic coordination conjugate was facilely synthesized using an efficient synthetic strategy in which Gd<sup>3+</sup> and Cu<sup>2+</sup> coordinated to their respective chelators, forming a strong complex to avoid trans-chelation or trans-metalation at physiological pH. The trimodal ligand can be further modified or functional groups introduced for biological applications.

### Nano-sized trimodal probes

To design PET-MR trimodality imaging probes, the nano-structures should have enough surface area to offer several conjugation sites for labeling three imaging modality reporters and other functionalities. Table 3 summarizes recently developed trimodal PET-MR and SPECT-MR probes.

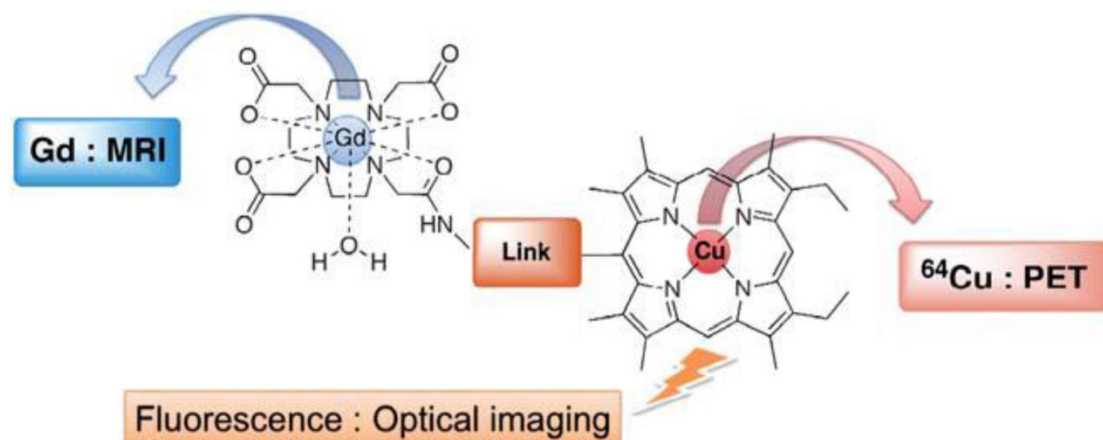


**Figure 16.** Small molecule trimodal probe. Adapted with permission from [97], copyright 2011 Royal Society of Chemistry.

**Table 3.** Trimodal probes and their applications.

Probe	PET(SPECT) reporter	MR reporter	Third imaging reporter	Applications	Ref.
Gd(DO3A-AM)- <sup>64</sup> Cu(Porphyrin)	<sup>64</sup> Cu	Gd-DO3A	Porphyrin fluorescence	Potential trimodal imaging	97
<sup>64</sup> Cu-Apoferretin (APF)	<sup>64</sup> Cu	APF/Fe <sup>3+</sup>	Fe <sup>3+</sup> and APF	HT29 tumor targeting	101
<sup>111</sup> In-DTPA-CLIO-Tat-FITC	<sup>111</sup> In	SPIO	FITC fluorescence	Tracking and recovery of progenitor cells	102
<sup>68</sup> Ga-HIV-1-tat-FITC peptide and <sup>111</sup> In-HIV-1-tat-FITC peptide	<sup>68</sup> Ga & <sup>111</sup> In	SPIO	FITC fluorescence	Hepatogenic HuH7 cells labeling	105
<sup>64</sup> Cu-DOTA-HSA-IONP-Cy5.5	<sup>64</sup> Cu	SPIO	Cy5.5 NIR fluorescence	Good retention rate and a high extravasation rate at tumor	106
<sup>124</sup> I-TCL-SPIONs	<sup>124</sup> I	SPION	<sup>124</sup> I Cerenkov radiation as optical	SLN imaging	107
<sup>68</sup> Ga-SPION	<sup>68</sup> Ga	SPION	<sup>68</sup> Ga Cherenkov optical	SLN imaging	108
<sup>68</sup> Ga{MNP@SiO <sub>2</sub> (NIR797)}	<sup>68</sup> Ga	CoFe <sub>2</sub> O <sub>4</sub>	NIR797 fluorescence	SLN imaging	109
<sup>67</sup> Ga-MNP@SiO <sub>2</sub> (RITC)-PEG/NH <sub>2</sub> -AS1411	<sup>67</sup> Ga	CoFe <sub>2</sub> O <sub>4</sub>	RITC fluorescence	Tracking cancer cells	112
<sup>64</sup> Cu-NOTA-Au-IONP-Affibody	<sup>64</sup> Cu	SPIO	Plasmonic Au optical	Targeting EGFR-positive tumor	116
<sup>64</sup> Cu-Fe-Ga-PEG	<sup>64</sup> Cu	Fe <sup>3+</sup>	PAT or NIR	Photothermal therapy	117
<sup>64</sup> Cu-DOTA-GdVO <sub>4</sub> :4%Eu-DGEA	<sup>64</sup> Cu	GdVO <sub>4</sub>	Eu-doped	Conjugate with Asp-Gly-Glu-Ala (DGEA) peptide for integrin α <sub>v</sub> β <sub>1</sub> targeted	121
<sup>64</sup> Cu-DOTA-MSN-Gd-DTTA-FITC	<sup>64</sup> Cu	Gd-DTTA	FITC fluorescence	Mapping of SLNs and tumor metastases	122
<sup>18</sup> F-NaYF <sub>4</sub> :Gd <sup>3+</sup> /Yb <sup>3+</sup> /Er <sup>3+</sup>	<sup>18</sup> F	Gd <sup>3+</sup> doping NaYF <sub>4</sub>	Yb <sup>3+</sup> and Er <sup>3+</sup> co-doped UCL imaging	cellular scale to whole-body imaging of small animal	123
<sup>124</sup> I-(cRGDyk)2-NaGdF <sub>4</sub> :Yb <sup>3+</sup> /Er <sup>3+</sup>	<sup>124</sup> I	NaGdF <sub>4</sub>	Yb <sup>3+</sup> /Er <sup>3+</sup> co-doped UCL imaging	α <sub>v</sub> β <sub>3</sub> integrin-expressing U87MG tumor cells and xenografted tumor models	124
<sup>18</sup> F/ <sup>64</sup> Cu-Co <sub>0.16</sub> Fe <sub>2.84</sub> O <sub>4</sub> @NaYF <sub>4</sub> :Yb <sup>3+</sup> /Er <sup>3+</sup> -BP-PEG	<sup>18</sup> F & <sup>64</sup> Cu	Co <sub>0.16</sub> Fe <sub>2.84</sub> O <sub>4</sub>	Yb <sup>3+</sup> /Er <sup>3+</sup> co-doped UCL imaging	SLN imaging	128

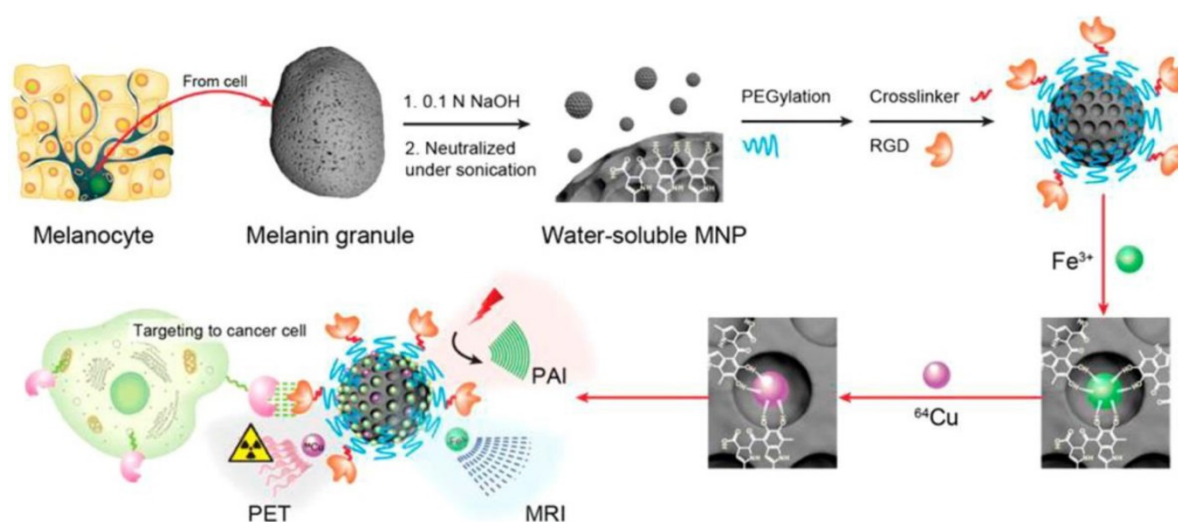


**Figure 17.** Multimodality molecular imaging of melanin nanoparticles. The melanin granules were first dissolved in 0.1 N NaOH aqueous solution, and then neutralized under sonication to obtain melanin nanoparticles with high water monodispersity and homogeneity. After PEG surface-modification, RGD was further attached to the MNP for tumor targeting. Then, Fe<sup>3+</sup> and/or <sup>64</sup>Cu<sup>2+</sup> were chelated to the obtained MNPs for PAI/MRI/PET multimodal imaging. Adapted with permission from [100], copyright 2014 American Chemical Society.

Melanin, oxidation from tyrosine, is a functional biomarker for melanoma imaging due to its abundance in melanotic melanomas. Interestingly, water-soluble melanin nanoparticles (MNPs) were reported as a multifunctional nanoplatform for PET-MR-photoacoustic imaging (PAI) (Figure 17) [100]. The advantages of MNPs include their intrinsic PAI characteristics and natural binding ability with metal ions such as <sup>64</sup>Cu<sup>2+</sup> and Fe<sup>3+</sup>, which could skip the complicated chelator conjugation. With further conjugation with cyclic c(RGDfC) peptide for  $\alpha_v\beta_3$  integrin targeting, MNPs showed high accumulation in U87MG tumor by the enhanced permeability and retention effect (EPR). However, the disadvantages of melanin multifunctional nanoplatforms such as their poor water-solubility, melanin aggregation into polymer, and metal ions-initiated precipitation need to be overcome for their further theranostic applications. Apoferritin was used as a nanoplatform to embed MNPs into its cavity as a trimodal imaging probe for efficient cancer targeting because of its transferrin receptors 1-targeting ability [101]. MNP as a trimodal imaging PET-MR-PAT nanoplatform showed it can be applied to imaging of diseased tissues at different depths with molecular and anatomical information. It can also serve as a platform for guiding tumor resection, in which PAI is used to localize the superficial and relatively deep tumors in surgery. The results indicated that MNP is promising for theranostic applications.

Functional SPIO nanoparticles meet the requirements to label PET/SPECT isotopes at conjugation sites, to attach functional groups as optical/NIR fluorescence imaging reporters, and even to conjugate targeting groups with receptor-binding

affinity. One pioneering work on functional SPIO nanoparticles as trimodal imaging probes is the novel trimodal SPIO nanoparticle CLIO-Tat, which consists of a monocrystalline MR-active Fe<sub>3</sub>O<sub>4</sub> core (5 nm) stabilized by an aminated dextran coating (45 nm) for *in vivo* tracking of progenitor cells [102] (Figure 18). The dextran coating was attached to lysine moieties of FITC-derivative Tat peptide for fluorescence imaging and also conjugated with DTPA chelator to label with <sup>111</sup>In for SPECT imaging. The probe could be used efficiently for *in vivo* tracking of the distribution and differentiation of progenitor and stem cells by the three imaging techniques. A similar strategy was developed by the same group to synthesize a new trimodal probe <sup>64</sup>Cu-TNP for imaging macrophages in inflammatory atherosclerotic plaques [103]. The aminated polysaccharide coating was used to optimize the biocompatibility, to extend the blood half-life, to attach the <sup>64</sup>Cu-labeled-DTPA for PET imaging and to conjugate fluorochrome for near-infrared imaging. *In vivo* PET studies on apoE<sup>-/-</sup> mice demonstrated higher uptake and longer persistence in the aortic arch for <sup>64</sup>Cu-TNP than for <sup>18</sup>F<sup>18</sup>FDG [104], which is consistent with fluorescence microscopy studies. The result indicated that microscopic tracer distribution could be evaluated for <sup>64</sup>Cu-TNP due to its higher radioactive signal in the aortic arch, an area of frequent inflammatory atherosclerotic plaques. Using aminosilane to modify the coating of SPIOs provided amino-reactive moieties, which have a positive charge and thus are favourable for linking with the fluorescent dye fluorescein isothiocyanate for cell tracking *in vivo* [105].

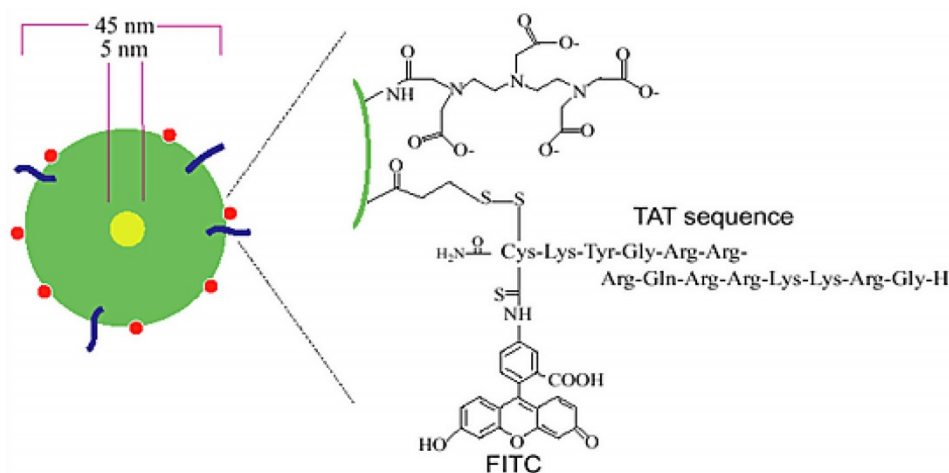


**Figure 18.** Schematic diagram of triple-labeled CLIO-Tat. The developed magnetic particle consists of a central superparamagnetic iron oxide core (yellow), sterically shielded by crosslinked dextran (green). The particle core measures ~5 nm and the overall particle size is 45 nm. The FITC-derivatized Tat peptide (blue) was attached to the aminated dextran, yielding an average four peptides per particle. The dextran surface was also modified with the chelator DTPA (red) for isotope labeling. Adapted with permission from [102], copyright 2000 Springer Publishing Ltd.

Dopamine was used to modify the surface of SPIO nanoparticles to increase their hydrophilicity so that the modified nanoparticles could be easily encapsulated into human serum albumin (HSA) matrices [106]. This approach of encapsulation by HSA is similar to that of encapsulation of drug molecules or drug loading. The resulting HSA-IONPs were conjugated with  $^{64}\text{Cu}$ -DOTA chelates and labeled with the fluorophore Cy5.5 as a trimodal PET-MR-NIRF probe for imaging the U87MG xenograft mouse model. To assess the pharmacokinetics of the probe and its preclinical applications, PET-MR-NIRF tri-modal imaging studies were performed through *in vivo*, *ex vivo*, and histological examinations. The HSA-IONPs demonstrated a long blood half-life and considerable tumor retention due to EPR. The *in vivo* studies showed that decomposition of HSA coating from the particle surface may occur, but the investigations using *ex vivo* fluorescence demonstrated that no substantial detached HSA was found. The results of this study indicated that the particles can be used as nanosystems for co-loading drug molecules, such as paclitaxel (PTX), for theranostic applications. Moreover, the HSA coating layer could enhance electrostatic interaction of the particles with drug molecules.

A very interesting approach for the preparation of a PET-MR-optical trimodal imaging probe is that of  $^{124}\text{I}$  radioisotope conjugation to SPIO nanoparticles. The trimodal nanoparticles exhibited a long half-life of 4.2 days. Their emission of high-energy positron decay with a  $\beta^+$  mean energy of 819 keV led to strong Cerenkov radiation as an optical imaging reporter in which no fluorescent dye is needed, unlike in the case of previously described trimodal imaging reporters

probes (Figure 19) [107]. SPION with cross-linked polymer coating layers containing PEG (TCL-SPION) was selected as an MR imaging reporter.  $^{124}\text{I}$  was labeled at the ortho-position of the phenol ring in tyramine (4-(2-aminoethyl)phenol) that modified the coating of  $\text{Fe}_3\text{O}_4$  magnetite nanoparticles to provide tyramine-conjugated TCL-SPIONs. The optimal particle size, high *in vivo* stability and anti-biofouling characteristics of TCL-SPIONs were suitable for SLN imaging. The  $^{124}\text{I}$ -labeled TCL-SPIONs were injected into both front paws of a 4T1 tumor-bearing BALB/c mouse. Cerenkov imaging, microPET and MR imaging consistently demonstrated a lower accumulation of  $^{124}\text{I}$ -labeled TCL-SPIONs in the left brachial SLN, while LN could be more accurately visualized in optical images than in the other two modality images. The lower uptake of the probe in the left brachial SLN that is close to the implanted 4T1 tumor was because of metastasis of the tumor cells into the LN, resulting in its dysfunction. Consistent results were also found in the *ex vivo* optical and microPET images of the dissected LNs. Similar to  $^{124}\text{I}$  radioisotope,  $^{68}\text{Ga}$  enables Cerenkov radiation that can be used as an optical imaging reporter. A single dose of  $^{68}\text{Ga}$ -SPIONs was reported as a PET-MR-Cerenkov trimodal probe for imaging and biodistribution study of SLNs [108].

MNP- $\text{SiO}_2$ (NIR797), magnetic silica nanoparticle encapsulating NIRF dye in a silica shell, was reported as a trimodal PET-MR-NIRF probe for *in vivo* imaging of the SLN in mice [109]. Due to encapsulation of NIR797 dye in a rigid silica matrix, enhanced fluorescence signal intensity and improved photostability of MNP- $\text{SiO}_2$ (NIR797) were found. The probe was used to visualize cells in the deep tissue by enhanced NIR fluorescence imaging. When the

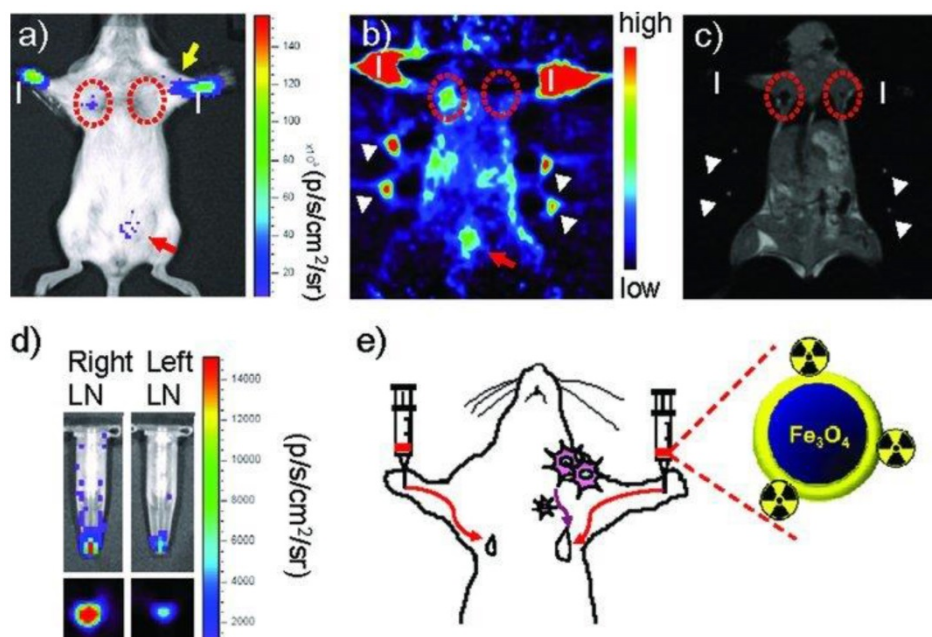


**Figure 19.** Triple-modality imaging of radiolabeled nanoparticles: a) optical, b) microPET, and c) MRI of  $^{124}\text{I}$ -labeled SPIONs injected into the front paws of a BALB/c mouse bearing a 4T1 tumor implanted on its shoulder. Tumor: yellow arrow; sentinel lymph node: red dotted circle; injection site: "I"; bladder: red arrow; fiducial markers: white arrow head. d) Ex vivo luminescence (top) and microPET (bottom) images of the dissected lymph nodes. e) Schematic diagram of the tumor metastasis model and injection route of radiolabeled nanoparticles. Adapted with permission from [107], copyright 2010 Wiley-VCH.

chelator NOTA was covalently conjugated to the surface of MNP-SiO<sub>2</sub>(NIR797) and radiolabeled with a radioisotope  $^{68}\text{Ga}$ , the fluorescence intensity and stability of the resulting  $^{68}\text{Ga}$ -{MNP-SiO<sub>2</sub>(NIR797)} did not change significantly. T2 relaxivity measurements on different magnetic field MR systems showed that radiolabeling of  $^{68}\text{Ga}$  did not interfere with the magnetic characteristics. For Gd-chelated macromolecule MR contrast agents, the particle size of G6 dendrimers (~9 nm) was more suitable for detection of LN than the particle sizes of G8 (~12 nm) or G4 (~6 nm) dendrimers [110]. For silica nanoparticles, the size of 40 nm among several particle sizes was reported to have an ideal distribution profile in lymphatics [111]. Nanoparticles with particle size  $45 \pm 6$  nm were selected for SLN imaging as they were optimal for entering the lymphatic vessels and retaining in the capillary vessels within the lymphatics. The trimodal tracer was injected into the forepaw of mice for SLN mapping using PET, MR and NIRF. When 100  $\mu\text{g}$  of  $^{68}\text{Ga}$ -{MNPSiO<sub>2</sub>(NIR797)} was subcutaneously injected, PET images of axillary and brachial LNs and clear signals of NIRF in axillary and brachial LNs could be obtained, but MR images in axillary LNs were detected only at doses higher than 200  $\mu\text{g}$  of  $^{68}\text{Ga}$ -{MNP-SiO<sub>2</sub>(NIR797)}. The strong fluorescence signal indicated that it could provide real-time NIRF imaging for intra-operative guidance. Similarly, encapsulation of fluorescent rhodamine with AS1411 aptamer, which targets nucleolin protein in cancer

cells, in a silica matrix of cobalt-ferrite magnetic nanoparticles was conjugated to  $^{67}\text{Ga}$ -labeled chelate for tracking cancer cells by *in vitro* and *in vivo* multimodal imaging techniques [112].

Unlike most PET-MR or multimodal probes, which have only one single component of SPIO nanoparticles, dumbbell-like NPs (DBNPs) have two different NPs within one nanostructure. The advantages of dumbbell nanostructure are that it offers different NP surfaces for coupling of several biological targeting moieties, drug molecules, or labeling imaging reporters for its applications in diagnosis and therapy that overcome the limitation of single component NP such as low yield of conjugating different ligands simultaneously, intimate interference of functional groups, complex imaging reporters labeling or modification, and poorer performance for *in vivo* investigations [113-115]. A highly monodisperse dumbbell-shaped AuIONP with a plasmonic Au as an optical imaging reporter was developed as a trimodal PET-MR-optical probe for cancer imaging [116]. The hetero-nanostructures have optimal physicochemical parameters such as size, shape, highly monodisperse characteristics and surface modification capability for application in tumor cell detection. In order to enhance the *in vivo* targeting ability of the nanoprobe toward epidermal growth factor receptor (EGFR)-positive tumors, affibody molecules were conjugated to the IO surface via PEG linkers and the Au component was surface-specifically modified with thiolated PEG

linkers to conjugate chelator NOTA, then radiolabeled with  $^{64}\text{Cu}$ , resulting in an EGFR-targeting PET-MR-optical imaging probe,  $^{64}\text{Cu}$ -NOTA-Au-IONP-Affibody. *In vitro* rapid cell uptake of  $^{64}\text{Cu}$ -NOTA-Au-IONP-Affibody in A431 cells showed high specificity for binding with EGFR positive cells. *In vivo* MR and PET imaging studies showed higher tumor accumulation of the nanoprobe, indicating its specific targeting to EGFR-expressing cells and tumor. The results indicated that the nanoplatform could be promising for conjugation with various types of biomolecules for cancer targeting or drug delivery through surface modifications.

Only one example of chelator-free radiolabeling of  $^{64}\text{Cu}$  to ultra-small iron-gallic acid coordination polymer nanoparticles as a trimodal probe has been reported [117]. *In vivo* MR and PAT bimodal imaging studies demonstrated passive tumor targeting of the PEGylated iron-gallic acid coordination polymer nanoparticles (Fe-Ga-PEG CPNs). Fe-Ga-PEG CPNs were used for further *in vivo* photothermal therapy. The  $^{64}\text{Cu}$ -radiolabeled Fe-Ga-PEG enabled *in vivo* PET imaging. The straightforward preparation and biocompatible characteristics of the trimodal probe indicated its promising theranostic application.

Besides SPIO-based nanoparticles, lanthanide-rich nanoparticles such as lanthanide-co-doped  $\text{NaYF}_4$  nanophosphors are another class of nanostructures recently developed as multimodal imaging probes. By doping  $\text{Gd}^{3+}$ ,  $\text{Yb}^{3+}$ , and  $\text{Er}^{3+}$  into  $\text{NaYF}_4$ , the resulting nanocrystals of  $\text{Gd}^{3+}/\text{Yb}^{3+}/\text{Er}^{3+}$  co-doped  $\text{NaYF}_4$  can be used as bimodal MR-luminescent imaging probe due to the unique magnetic and luminescent properties of these lanthanide ions [118-120]. A PET-MR-fluorescence imaging probe for targeting integrin  $\alpha_2\beta_1$  was composed of  $^{64}\text{Cu}$ -labeled  $\text{Eu}^{3+}$ -doped  $\text{GdVO}_4$  conjugated with Asp-Gly-Glu-Ala (DGEA) peptides, forming two-dimensional nanosheets [121]. The oleic acid (OA)-coated  $\text{Eu}^{3+}$ -doped  $\text{GdVO}_4$  nanosheets were prepared by a solvothermal reaction, then OA was replaced by polyacrylic acid (PAA) via ligand exchange to improve the biocompatibility. The resulting carboxyl-functionalized nanosheets were further conjugated with DOTA for  $^{64}\text{Cu}$  labeling and with DGEA for integrin  $\alpha_2\beta_1$  targeting. *In vitro* fluorescence imaging and *in vivo* MR and micro-PET imaging studies in a small animal prostate cancer model of  $^{64}\text{Cu}$ -labeled  $\text{Eu}^{3+}$ -doped  $\text{GdVO}_4$  nanosheets demonstrated their good optical property, T1-weighted MR signal enhancement and integrin  $\alpha_2\beta_1$  targeting. A mesoporous silica-based trimodal imaging nanoprobe (MSN-probe), which is comprised of three imaging reporters including NIR dye ZW800, T1 MR contrast agent  $\text{Gd}^{3+}$  and PET radionuclide  $^{64}\text{Cu}$

coordinated to chelators in a mesoporous silica-based nanoparticle via various conjugation steps, was reported to accomplish long-term *in vivo* SLNs imaging [122]. Due to its high stability and intracellular retention, accumulation of the nanoprobe in metastatic T-SLNs and normal contra-lateral SLNs (N-SLNs) in a 4T1 tumor metastasis model could be distinguished.

$^{18}\text{F}$ -labeled lanthanide nanocrystals of  $\text{Gd}^{3+}/\text{Yb}^{3+}/\text{Er}^{3+}$  co-doped  $\text{NaYF}_4$  was developed for trimodal PET-MR-optical imaging in which lanthanide-doped nanocrystals provide MR and luminescence imaging reporters, while  $^{18}\text{F}$  radiolabeling simultaneously enables PET imaging [123]. Hydrophobic OA-coated  $\text{NaY}_{0.2}\text{Gd}_{0.6}\text{Yb}_{0.18}\text{Er}_{0.02}\text{F}_4$  nanophosphors (OA-NPs) were replaced by hydrophilic citrate-capping (cit-NPs) through ligand exchange of OA with citrate.  $^{18}\text{F}$ -radiolabeling was achieved by a reaction through the strong binding between  $\text{Y}^{3+}$  and  $^{18}\text{F}$ . RGD peptide-functionalized  $\text{Yb}^{3+}/\text{Er}^{3+}$  co-doped  $\text{NaGdF}_4$  upconversion nanophosphors (UNCNPs) were employed as a trimodal probe for tumor angiogenesis imaging [124]. The octalamine-modified polyacrylic acid polymer coating was replaced with PEG polymers and conjugated with dimeric cyclic RGD peptides (cRGDyk) $_2$  to increase the specific binding ability. The resulting (cRGDyk) $_2$ -conjugated nanophosphors were radiolabeled with  $^{124}\text{I}$  at the tyrosine moiety of (cRGDyk) $_2$  peptides through a radioiodination method (Figure 20). RGD peptides specifically bind to  $\alpha_v\beta_3$  integrin, which is overexpressed in many types of cancer and vasculature. RGD-functionalized UNCNPs  $^{124}\text{I}$ -(cRGDyk) $_2$ -UNCNPs were reported as an integrin-positive U87MG tumor-specific targeted trimodal probe. Specific localization of (cRGDyk) $_2$ -UNCNPs on the surface of U87MG cells by luminescence imaging, positive T1 contrast enhancement in U87MG tumors by MRI and specific uptake of  $^{124}\text{I}$ -(cRGDyk) $_2$ -UNCNPs in U87MG tumors by PET demonstrated that the probe can be used in trimodal imaging for cancer-specific diagnosis. Although the preliminary *in vitro* cellular cytotoxicity of (cRGDyk) $_2$ -UNCNPs was low, *in vivo* toxicity including histological and metabolic toxic effects needs to be established. Potential toxicity of unchelated lanthanide-containing nanoparticles remains an obstruction for their further applications in preclinical and clinical investigations.

Fabrication of hybrid inorganic nanocomposites, which contain two or more components for multimodal imaging reporters, is a novel approach to synthesize multimodal imaging probes. SPIOs such as  $\text{Fe}_3\text{O}_4$  have been used as a MR imaging reporter, while

lanthanide-rich nanomaterials such as  $\text{NaGdF}_4$  or lanthanide co-doped nanophosphors represent the luminescence imaging reporter in hybrid inorganic nanoparticles.  $\text{Fe}_3\text{O}_4@ \text{NaGdF}_4$  nanoparticles [125],  $\text{NaYF}_4@ \text{Fe}_x\text{O}_y$  [126], and  $\text{Fe}_3\text{O}_4@ \text{LnF}_{3,24}$  [127] were reported as bimodal MR and optical imaging probes. When radiolabeling with  $[^{18}\text{F}]$ -fluoride or  $^{64}\text{Cu}$ -/ $^{99\text{m}}\text{Tc}$ - biphosphonate (BP) conjugates to  $\text{Fe}_3\text{O}_4@ \text{NaYF}_4$  core/shell nanoparticles with different cation dopants in the shell or core, the inorganic core-shell nanoparticles were applied as trimodal probes for imaging SLN [128]. Before radiolabeling, the nanoparticles were coated with BP-PEG to improve their binding to  $[^{18}\text{F}]$ -fluoride or  $^{64}\text{Cu}$ -/ $^{99\text{m}}\text{Tc}$ -biphosphonate conjugates. High  $r_2$  values and  $r_2/r_1$  ratios for T2-weighted MRI were found for both  $\text{Co}_{0.16}\text{Fe}_{2.84}\text{O}_4@ \text{NaYF}_4(\text{Yb}, \text{Er})$ -BP-PEG and  $\text{Fe}_3\text{O}_4@ \text{NaYF}_4(\text{Yb}, \text{Tm})$ -BP-PEG. The metabolism from PET-MR imaging showed positively charged  $\text{Fe}_3\text{O}_4@ \text{NaYF}_4(\text{Yb}, \text{Tm})$ -BP-PEG were excreted from the blood pool faster than negatively charged  $\text{Co}_{0.16}\text{Fe}_{2.84}\text{O}_4@ \text{NaYF}_4(\text{Yb}, \text{Er})$ -BP-PEG. *In vivo* imaging studies in LNs showed obvious advantages of combining imaging modalities (**Figure 21**). When combined with highly sensitive PET, but not MRI alone, the *in vivo* imaging studies offered improved presurgical mapping of iliac and popliteal LN locations and provided more details to interpret the imaging of SLNs that are relevant to the pathology of LNs and tumor metastasis in humans. The fluorescence could offer additional information of

anatomical and functional changes during surgery and subsequently during pathological examination of excised tissues.

## Discussion

Thanks to recently available hybrid imaging techniques, the advantages of high temporal and spatial sensitivity, and the anatomical and functional information provided by both PET and MR imaging techniques can be obtained by combination of the single imaging modalities. With the injection of a multimodal probe, both the scanning time and dose can be reduced with enhanced imaging signals for diagnosis, tumor differentiation, localisation and mapping, etc. Significant differences in concentrations of the two imaging probes should be noted due to the large differences in sensitivities of the two techniques. PET tracers generally need to be injected in extremely small concentrations (pico-nano-molar range), whilst MR CAs need to be injected in millimolar range, typically in thousand-fold higher concentrations than PET tracers. This problem cannot be solved by simply adding two different classes of imaging probes together. Individual PET tracer and MR CAs could be injected simultaneously, but validation and registration problems could arise unless they have identical pharmacodynamic properties. The development of multimodal probes enables simultaneous data acquisition without validation and registration problems.

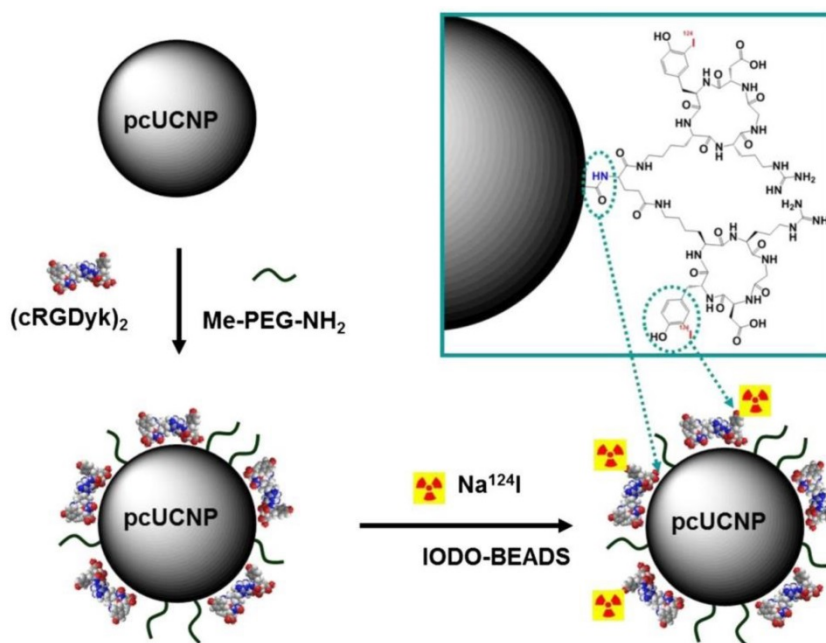


**Figure 20.** Synthesis scheme of  $^{124}\text{I}$ -(cRGDyk) $_2$ -UCNP conjugates. Polymer-coated UCNP (pcUCNP) was reacted both with (cRGDyk) $_2$  peptide and with MeO-PEGNH $_2$  (molecular weight, 2,000) using EDC/Nhydroxysulfosuccinimide. Tyrosine residues of (cRGDyk) $_2$  were labeled with  $^{124}\text{I}$  using Iodo-Beads (Pierce). Adapted with permission from [124], copyright 2013 Society of Nuclear Medicine and Molecular Imaging.

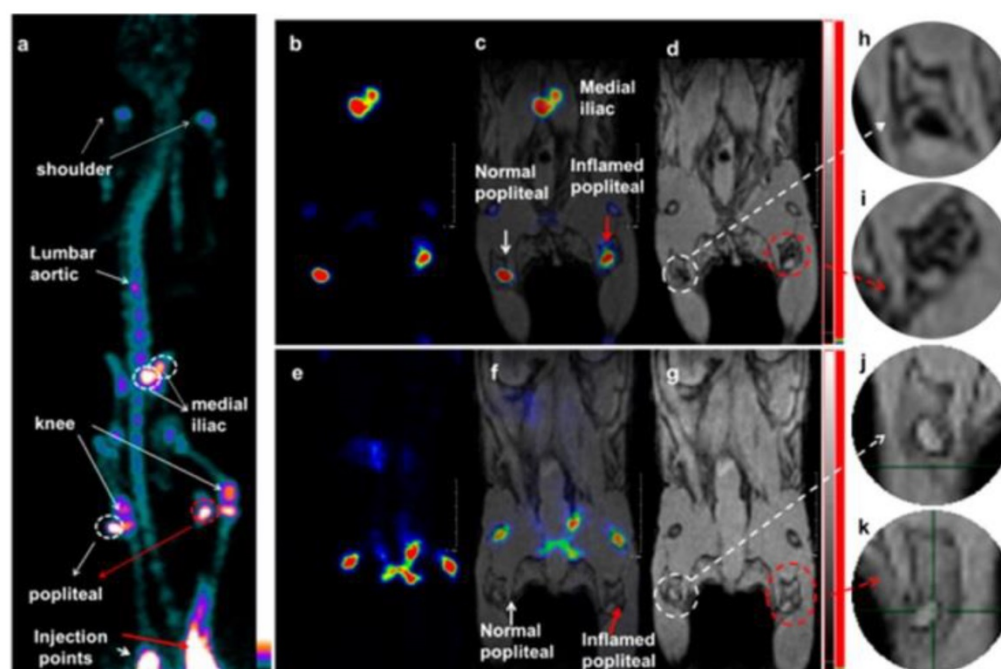


**Figure 21.** Lymph node PET-MRI imaging of a mouse with an inflamed right leg using  $^{18}\text{F}$ -labeled  $\text{Fe}_3\text{O}_4@/\text{NaYF}_4(\text{Yb, Tm})\text{-BP-PEG NPs}$  (a-d) or with  $^{18}\text{F}$ -fluoride only (e-g): (a) whole-body PET image showing uptake of radiolabeled NPs (maximum intensity projection; bone uptake was observed due to gradual release of fluoride from NPs due to the 7 h delay post injection of NPs); (b) PET image showing popliteal and iliac lymph nodes (coronal section); (c) PET-MRI fused image (coronal section); (d) MR image (coronal section) with darkening contrast inside the popliteal lymph node at left-rear (white circle) and “outside” lymph node at the inflamed right-rear (red circle) induced by injection of  $30\ \mu\text{L}$   $0.67\ \text{mg/mL}$  lipopolysaccharide (LPS) 18 h prior to imaging, and at iliac lymph node; (e) PET image following injection of  $^{18}\text{F}$ -fluoride showing no contrast in lymph nodes in the absence of NPs and prominent uptake by skeleton; (f) PET-MRI fused image following injection of  $^{18}\text{F}$ -fluoride, showing no radioactivity associated with lymph nodes; (g) MR image showing no difference between normal popliteal lymph node at left-rear (white circle) and the inflamed lymph node at right-rear leg induced by injection of  $30\ \mu\text{L}$   $0.67\ \text{mg/mL}$  LPS 18 h prior to imaging; and (h-k) enlarged MR images of corresponding lymph nodes. Adapted with permission from [128], copyright 2016 American Chemical Society.

Nano-structured multimodal probes have their advantages for diagnosis of tumors, SLN metastasis, and inflammatory disease, etc. Compared with nano-structures, small molecules are unlikely to be designed as multimodal imaging probes due to their limited loading capacity. Despite these limitations, small molecular probes have their applications for certain biological events such as pH-response, in which the MR reporter relaxivity is responsive to pH while the PET reporter is responsible for sensitivity and quantification. The limited loading capacity of a small molecule accounts for it being unlikely to be a carrier of trimodal imaging reporters and functionalities. There is only one example of a trimodal imaging probe reported as a proof-of-concept of this design [97]. The majority of multi-imaging modal probes are nanoparticle-based because of their large surface area for conjugation sites, targeting and therapeutic biomolecules functionalizations, and physicochemical and biological stability.

CNTs have been used as nano-carriers for diversified biomedical applications due to their characteristics such as high surface area, nanoscale tube with hollow cavity, etc [76]. By incorporating imaging probes into CNTs, CNTs are promising

candidates for multimodal imaging through chemical design to improve their sensitivity, biocompatibility and pharmacokinetics for diagnostic and therapeutic applications, although their potential cytotoxicity needs to be taken into account [77-84]. Hybrid nanostructures can be formed from non-covalent functionalization either in the cavity or external attachment, for example, functionalization with phospholipid-PEG for better biocompatibility in human serum environments. The length of hybrid carbon nanotube imaging probes is crucial for their biodistribution profile. Liposomes are another class of nano-vehicles to deliver tumor-targeting antibody or peptide together with conjugated multimodal imaging reporters for cancer imaging and therapy due to their biocompatibility, high probe-to-carrier loading ratios, and straightforward encapsulation capability of both hydrophilic and hydrophobic probes [88-91]. There is a challenge to achieve precise control of loading multiple functionalities. Bioconjugation methodologies of functional groups or specific targeting moiety modifications on the surface of nanostructures without composition control could hinder their translational applications. Moreover, the synthesis methodology for preparing nanostructures as multimodal imaging probes may have its

challenges as steps in the synthesis may interfere with each other. Intramolecular interference between imaging reporters and targeting groups in a single entity may reduce its targeting capability or change the biodistribution pattern of the probe. Ferritin nanocages as a nanoplatform for multifunctional loading with precise control of their composition would be a promising way [129].

The size, shape, composition, coating, and surface properties of the nanostructures play important roles in the biodistribution of the multimodal probes. Larger particles of dextran-coated nanoparticles lead to more liver uptake. Quick uptake of SPIO nanoparticles by macrophages of the MPS could lead to short circulation times, which could hinder further conjugation with targeting moieties. PEGylation of the nanoparticle surface makes imaging probes biocompatible: the hydrophilic layer could minimize particle aggregation and MPS uptake. PEG-coating causes the nanoparticles to have a longer blood circulation time to improve uptake in LNs and increased accumulation in tumor [130]. Modification of the surface of SPIOs with dopamine could increase the hydrophilicity of nanoparticles, which is favourable for encapsulation into HSA matrices [106]. Cell viability studies showed that most of radiolabeled SPIOs and other multimodal imaging probes did not have cellular toxicity in a variety of cell lines. However, the *in vivo* toxicity profiles of imaging probes through a well-designed toxicity test need to be established for preclinical investigations and before clinical trials.

The size of nanostructures is one of the most important factors for the biodistribution pattern of the imaging probe. For nanoparticles, a small hydrodynamic size (less than 100 nm) and low zeta potential have an important effect on controlling circulation time. Avoiding immediate MPS clearance is favourable for targeting applications [131]. The accumulation of 100 nm particles in the MPS was much higher compared with larger particles [132]. Smaller particles had much higher and faster uptake in the target of interest, while larger nanoparticles transported more slowly to the target [128]. Smaller particles also have higher tumor uptake [133,134], and the multimodal probe could be made as small as possible for tumor targeting.

The majority of radiometals suitable for PET/SPECT imaging and therapy applications need a chelator to form stable complexes [135]. A specific coordination chelator has been employed for each particular radiometal based on its physicochemical properties such as oxidation state, coordination number, kinetic inertness, etc. The chelator also has its second function to covalently bind to the targeting

moiety of the probe for its biological applications, defined as bifunctional characteristics. The transition metals such as  $^{64}\text{Cu}$ ,  $^{68}\text{Ga}$ ,  $^{99\text{m}}\text{Tc}$  form tetradentate to hexadentate chelates, as commonly seen in radiopharmaceuticals, while the lanthanides such as  $\text{Gd}^{3+}$  tend to form eight to nine coordination complexes for T1-weighted MRI contrast agents. Although the well-established radiometal chelation is the common radiochemical method to label nanoparticles, there are some shortcomings such as unfavorable radiolabeling conditions [136], and transchelation of radiometal to proteins leading to high uptake in nontargeted organs and further misinterpretation of PET images [137-139]. Chelator-free and core-doped radiolabeling are new approaches to radiolabel nanoparticles with (1) improved stability, which is critical for diagnostic accuracy, (2) increased radiolabeling yield by straightforward attachment of radionuclides to the nanoparticle surface or incorporation into the particle core, and (3) better *in vivo* performance due to no transchelation of radiometal for misinterpretation of PET images and non-necessary radiation burden. However, the chelator-free and core-doped approaches lack general labeling procedures. Radiolabeling usually occurs before nanoparticle fabrication, which is another drawback. As such, incorporation of the radiometals during nanoparticle fabrication is not feasible for many short-lived radionuclides such as  $^{68}\text{Ga}$  [140]. Core-doping radiolabels during nanoparticle synthesis represents a general strategy for incorporating different metal radionuclides, but it needs full preparation and characterization of the entire nanoparticle for each radiosynthesis.

One of the key applications for multimodal imaging probes is to develop a probe by molecular design with targeting capability such as tumor, SLNs and fibrin targeting. By surface modifications or conjugation with targeting biomolecules, radiolabeled SPIO nanoparticles can be developed as targeted multimodal imaging probes, targeting, for example, hepatocytes with lactobionic acid [54], macrophages with maleic anhydride [55, 56], HT-29 cancer cells with oleonic acid [57], prostate-specific membrane antigen with glutamate-urea-lysine [58], MUC-1-positive breast cancer cells with monoclonal antibody C595 mAb [59], and fibrin for imaging of thrombus [92-94].

A variety of nanostructures have been used for imaging of cancer and therapy. Tumor uptake of imaging probe is either through EPR to tumor in a passive way or transport of nanoscale hydrophilic biomolecules via endocytosis for cellular internalization [141,142]. RGD has been chosen

extensively for preparing multimodal imaging probes due to its high affinity to tumor via integrin  $\alpha_v\beta_3$  expression [51-57]. The tumor-targeting peptide  $^{64}\text{Cu}$ -DOTA-IO-RGD is noted for having the highest *in vivo* tumor uptake ( $10.1 \pm 2.1$  %ID/g at 4 h post injection) among other targeting biomolecules. SPIOs radiolabeled with  $^{64}\text{Cu}$  or  $^{68}\text{Ga}$  and conjugated with engineered mAb also showed high tumor uptake. However, in some cases, *in vivo* targeting ability would be affected due to coverage of the targeting sites by protein corona [59].

Surgical removal of SLNs is an effective way to prevent tumor metastasis via the lymphatic system. SPIO nanoparticles have been used to detect SLNs with high spatial resolution [143]. However, using MRI only could lead to issues of quantification of probes with low specificity. So, adding a radiolabeled nuclide to SPIOs for combining high-sensitivity PET/SPECT with high-resolution MR to detect SLNs would be more accurate and could be quantified. Radiolabeled SPIOs as bimodal probes were reported for potential clinical applications in the preoperative localization and characterization of SLNs [41,42, 107,108]. Magnetic silica nanoparticles encapsulating NIRF dye in a silica shell MNP-SiO<sub>2</sub>(NIR797) is another class of multimodal probe for *in vivo* imaging of the SLN with enhanced fluorescence signal intensity and improved photostability due to encapsulation of NIR797 dye in a rigid silica matrix [109-112]. But, these reported imaging probes have only been used in preclinical proof-of-concept studies. No clinical trial data has been obtained.

## Conclusions

The goal of PET-MR and SPECT-MR multimodal probe development is to develop probes that have the following characteristics: high temporal and spatial sensitivity, anatomical and functional resolution, optimal biodistribution and pharmacokinetic profiles and specific targeting to the tissue of interest. The demand for new PET-MR and SPECT-MR multimodal probes is expected to increase to achieve these goals. There is a unique need to develop PET-MR and SPECT-MR multimodal probes for accurate diagnosis. The present review provides a comprehensive overview of all reported PET-MR and SPECT-MR multimodal probes including small molecule bimodal probes, nano-sized bimodal probes, small molecule trimodal probes and nano-sized trimodal imaging probes. The development of bimodal probes has advantages for simultaneous data acquisition and mapping of probes across resolution scales. The design and methodology of bimodal probes would result in various biological applications such as diagnosis of tumors, SLN metastases, and

inflammatory disease, etc. Through this comprehensive review, we aim to overview the current development of PET-MR and PET-SPECT bimodality probes in this new emerging field. Some multimodal probes can be extended to theranostic applications such as melanin nanoparticle (MNP) trimodal PET-MR-PAT probes. We believe more and more theranostic probes will be developed. Their novel synthetic methodologies, biocompatibility and potential applications, especially for tumor and SLNs have been surveyed, whereas the challenges as well as limitations of multimodal probes have been discussed. This review could provide some future research directions to those who have expertise in bio-imaging research such as medicinal chemistry and radiochemistry, PET/SPECT-MR physics, biology, radiology and biomedical imaging engineering.

## Abbreviations

BP: bisphosphonate; CA: contrast agent; CL: control-liposome; CNT: carbon nanotube; CPN: coordination polymer nanoparticle; CT: computed tomography; DBNP: dumbbell-like nanoparticle; DGEA: Asp-Gly-Glu-Ala peptide; DFO: desferrioxamine; DOTA: 1,4,7,10-tetraazacyclododecane-1,4,7,10-tetraacetic acid; DOTAGA: 1,4,7,10-tetraazacyclododecane-1-glutaric anhydride-4,7,10-triacetic acid; DPA: dipicolylamine-alendronate; DTCBP: dithiocarbamate bisphosphonates; DTPA: diethylenetriamine-pentaacetic acid; EGFR: epidermal growth factor receptor; EPR: enhanced permeability and retention effect; FDA: food and drug administration; FDG: fluorodeoxyglucose; FH: feraheme; fMRI: functional magnetic resonance imaging; HSA: human serum albumin; IO: iron oxide; LN: lymph node; LP: liposome; mAbMB: anti-mesothelin antibody; MAL: maleimide; MNP: melanin nanoparticle; MPS: mononuclear phagocyte system; MR: magnetic resonance; MRI: magnetic resonance imaging; MRS: magnetic resonance spectroscopy; MWNT: multi-walled carbon nanotube; NIR: near infrared; NODAGA: (2,2'-(7-(1-carboxy-4-((2,5-dioxopyrrolidin-1-yl)oxy)-4-oxobutyl)-1,4,7-triazonan e-1,4-diyl)diacetic acid; NOTA: 1,4,7-Triazacyclononane-1,4,7-triacetic acid; OL: octreotide-liposome; OA: oleic acid; PAA: poly(acrylic acid); PAI: photoacoustic imaging; PASP: polyaspartic acid; PAT: photoacoustic tomography; PEG: poly(ethylene glycol); PET: positron emission tomography; PTX: paclitaxel; RGD: cyclic arginine-glycine-aspartic; RF: radiofrequency; SA: serum albumin; SCN-Bz: S-2-(4-isothiocyanatobenzyl); SLN: sentinel lymph node; SPECT: single photon emission computed tomograph;

SPIO: superparamagnetic iron oxide; SRP: small and rigid platform; SSTR2: somatostatin receptor subtype 2; UCL: upconversion luminescence; UNCP: upconversion nanophosphor; USPIO: ultrasmall superparamagnetic iron oxide.

## Acknowledgements

Authors acknowledge the support from Lee Kong Chian School of Medicine, Nanyang Technological University Singapore (NTU) Start-Up Grant, Singapore and NTU Austrian Institute of Technology & Medical University of Vienna internal grant (NAM/15005), Singapore.

## Competing Interests

The authors have declared that no competing interest exists.

## References

- Mankoff DA. A definition of molecular imaging. *J Nucl Med.* 2007; 48(N): 18-21.
- Markus R. Molecular imaging: basic principles and applications in biomedical research. World Scientific. 2013.
- Massoud TF, Gambhir SS. Molecular imaging in living subjects: seeing fundamental biological processes in a new light. *Genes Dev.* 2003; 17: 545-80.
- Louie A. Multimodality imaging probes: design and challenges. *Chem Rev.* 2010; 110: 3146-95.
- Masters BR. Molecular Fluorescence: Principles and Applications. *J Biomed Opt.* 2013; 18: 039901.
- Phelps ME. Positron emission tomography provides molecular imaging of biological processes. *Proc Natl Acad Sci U S A.* 2000; 97: 9226-33.
- Paans AMJ, van Waarde A, Elsinga PH, Willemsen ATM, Vaalburg W. Positron emission tomography: the conceptual idea using a multidisciplinary approach. *Methods.* 2002; 27: 195-207.
- Beyer T, Townsend DW, Brun T, Kinahan PE, Charron M, Roddy R, et al. A combined PET/CT scanner for clinical oncology. *J Nucl Med.* 2000; 41: 1369-79.
- Merbach AS, Helm L, Toth E. The chemistry of contrast agents in medical magnetic resonance imaging. John Wiley & Sons. 2013.
- Caravan P, Ellison JJ, McMurry TJ, Lauffer RB. Gadolinium(III) chelates as MRI contrast agents: Structure, dynamics, and applications. *Chem Rev.* 1999; 99: 2293-352.
- Aime S, Botta M, Terreno E. Gd(III)-based contrast agents for MRI. *Adv Inorg Chem.* 2005; 57: 173-237.
- Beyer T, Townsend DW, Blodgett TM. Dual-modality PET/CT tomography for clinical oncology. *Q J Nucl Med.* 2002; 46: 24-34.
- Pichler BJ, Judenhofer MS, Pfannenbergl C. Multimodal Imaging Approaches: PET/CT and PET/MRI. *Molecular Imaging I: Springer.* 2008; 185 (Pt 1):109-132.
- Alessio AM, Kinahan PE, Cheng PM, Vesselle H, Karp JS. PET/CT scanner instrumentation, challenges, and solutions. *Radiol Clin North Am.* 2004; 42(vii): 1017-32.
- Bulte JWM, Kraitchman DL. Monitoring cell therapy using iron oxide MR contrast agents. *Curr Pharm Biotechnol.* 2004; 5: 567-84.
- Tyszka JM, Fraser SE, Jacobs RE. Magnetic resonance microscopy: recent advances and applications. *Curr Opin Biotechnol.* 2005; 16: 93-9.
- Sauter AW, Wehr HF, Kolb A, Judenhofer MS, Pichler BJ. Combined PET/MRI: one step further in multimodality imaging. *Trends Mol Med.* 2010; 16: 508-15.
- Jacobs RE, Cherry SR. Complementary emerging techniques: high-resolution PET and MRI. *Curr Opin Neurobiol.* 2001; 11: 621-9.
- Pichler BJ, Kolb A, Nagele T, Schlemmer HP. PET/MRI: paving the way for the next generation of clinical multimodality imaging applications. *J Nucl Med.* 2010; 51: 333-6.
- Jennings LE, Long NJ. 'Two is better than one' – probes for dual-modality molecular imaging. *Chem Commun.* 2009: 3511-24.
- Cai W, Chen X. Multimodality molecular imaging of tumor angiogenesis. *J Nucl Med.* 2008; 49 Suppl 2: 113S-28S.
- Seibold U, Wangler B, Schirmacher R, Wangler C. Bimodal imaging probes for combined PET and Ol: recent developments and future directions for hybrid agent development. *Biomed Res Int.* 2014: 153741.
- Bouziotis P, Psimadas D, Tsotakos T, Stamopoulos D, Tsoukalas C. Radiolabeled iron oxide nanoparticles as dual-modality SPECT/MRI and PET/MRI agents. *Curr Top Med Chem.* 2012; 12: 2694-702.
- de Rosales RT. Potential clinical applications of bimodal PET-MRI or SPECT-MRI agents. *J Labelled Comp Radiopharm.* 2014; 57: 298-303.
- Lahooti A, Sarkar S, Laurent S, Shanehsazzadeh S. Dual nano-sized contrast agents in PET/MRI: a systematic review. *Contrast Media Mol Imaging.* 2016; 11: 428-47.
- Frullano L, Catana C, Benner T, Sherry AD, Caravan P. Bimodal MR-PET agent for quantitative pH imaging. *Angew Chem Int Ed.* 2010; 49: 2382-4.
- Newell K, Franchi A, Pouyssegur J, Tannock I. Studies with glycolysis-deficient cells suggest that production of lactic acid is not the only cause of tumor acidity. *Proc Natl Acad Sci U S A.* 1993; 90: 1127-31.
- Suchý M, Bartha R, Hudson RH. "Click" chemistry toward bis (DOTA-derived) heterometallic complexes: potential bimodal MRI/PET (SPECT) molecular imaging probes. *RSC Advances.* 2013; 3: 3249-59.
- Vologdin N, Rolla GA, Botta M, Tei L. Orthogonal synthesis of a heterodimeric ligand for the development of the Gd(III)-Ga(III) ditopic complex as a potential pH-sensitive MRI/PET probe. *Org Biomol Chem.* 2013; 11: 1683-90.
- Notni J, Herrmann P, Dregely I, Wester HJ. Convenient synthesis of <sup>68</sup>Ga-labeled gadolinium (III) complexes: Towards bimodal responsive probes for functional imaging with PET/MRI. *Chem Eur J.* 2013; 19: 12602-6.
- Gianolio E, Maciocco L, Imperio D, Giovenzana GB, Simonelli F, Abbas K, et al. Dual MRI-SPECT agent for pH-mapping. *Chem Commun.* 2011; 47: 1539-41.
- Jarrett BR, Gustafsson B, Kukis DL, Louie AY. Synthesis of <sup>64</sup>Cu-labeled magnetic nanoparticles for multimodal imaging. *Bioconjugate Chem.* 2008; 19: 1496-504.
- Glaus C, Rossin R, Welch MJ, Bao G. In vivo evaluation of <sup>64</sup>Cu-labeled magnetic nanoparticles as a dual-modality PET/MR imaging agent. *Bioconjugate Chem.* 2010; 21: 715-22.
- Pluim JP, Maintz JA, Viergever MA. Image registration by maximization of combined mutual information and gradient information. *Med Image Comput Assist Interv.* Springer. 2000;19(8) : 452-61.
- Yang X, Hong H, Grailer JJ, Rowland JJ, Javadi A, Hurley SA, et al. cRGD-functionalized, DOX-conjugated, and <sup>64</sup>Cu-labeled superparamagnetic iron oxide nanoparticles for targeted anticancer drug delivery and PET/MR imaging. *Biomaterials.* 2011; 32: 4151-60.
- Aryal S, Key J, Stigliano C, Landis MD, Lee DY, Decuzzi P. Positron emitting magnetic nanoconstructs for PET/MR imaging. *Small.* 2014; 10: 2688-96.
- Deng SM, Zhang W, Zhang B, Hong RY, Chen Q, Dong JJ, et al. Radiolabeled cyclic arginine-glycine-aspartic (RGD)-conjugated iron oxide nanoparticles as single-photon emission computed tomography (SPECT) and magnetic resonance imaging (MRI) dual-modality agents for imaging of breast cancer. *J Nanopart Res.* 2015; 17: 19.
- Natarajan A, Xiong CY, Gruettner C, DeNardo GL, DeNardo SJ. Development of multivalent radioimmunonanoparticles for cancer imaging and therapy. *Cancer Biother Radiopharm.* 2008; 23: 82-91.
- Natarajan A, Gruettner C, Ivkov R, DeNardo GL, Mirick G, Yuan A, et al. NanoFerrite particle based radioimmunonanoparticles: binding affinity and in vivo pharmacokinetics. *Bioconjugate Chem.* 2008; 19: 1211-8.
- Lee H-Y, Li Z, Chen K, Hsu AR, Xu C, Xie J, et al. PET/MRI dual-modality tumor imaging using arginine-glycine-aspartic (RGD)-conjugated radiolabeled iron oxide nanoparticles. *J Nucl Med.* 2008; 49: 1371-9.
- Choi JS, Park JC, Nah H, Woo S, Oh J, Kim KM, et al. A hybrid nanoparticle probe for dual-modality positron emission tomography and magnetic resonance imaging. *Angew Chem Int Ed.* 2008; 47: 6259-62.
- Yang BY, Moon SH, Seelam SR, Jeon MJ, Lee YS, Lee DS, et al. Development of a multimodal imaging probe by encapsulating iron oxide nanoparticles with functionalized amphiphiles for lymph node imaging. *Nanomedicine (Lond).* 2015; 10: 1899-910.
- Misri R, Meier D, Yung AC, Kozlowski P, Hafeli UO. Development and evaluation of a dual-modality (MRI/SPECT) molecular imaging bioprobe. *Nanomedicine.* 2012; 8: 1007-16.
- de Rosales RTM, Tavares R, Paul R. Synthesis of <sup>64</sup>Cu (II)-bis (dithiocarbamate-bisphosphonate) and conjugation with superparamagnetic iron oxide nanoparticles: in vivo evaluation as dual-modality PET-MRI agent. *Angew Chem Int Ed.* 2011; 50: 5509-13.
- Cui XJ, Belo S, Kruger D, Yan Y, de Rosales RTM, Jauregui-Osoro M, et al. Aluminium hydroxide stabilised MnFe<sub>2</sub>O<sub>4</sub> and Fe<sub>3</sub>O<sub>4</sub> nanoparticles as dual-modality contrasts agent for MRI and PET imaging. *Biomaterials.* 2014; 35: 5840-6.
- Madru R, Kjellman P, Olsson F, Wingardh K, Ingvar C, Stahlberg F, et al. <sup>99m</sup>Tc-labeled superparamagnetic iron oxide nanoparticles for multimodality SPECT/MRI of sentinel lymph nodes. *J Nucl Med.* 2012; 53: 459-63.
- Locatelli E, Gil L, Israel LL, Passoni L, Naddaka M, Pucci A, et al. Biocompatible nanocomposite for PET/MRI hybrid imaging. *Int J Nanomedicine.* 2012; 7: 6021-33.
- Shanehsazzadeh S, Lahooti A. Biodistribution of 80 nm iron oxide nanoparticles labeled with <sup>99m</sup>Tc in Balb/c mice. *Nucl Med Biol.* 2014; 41: 625.
- Shanehsazzadeh S, Oghabian MA, Doha FJ, Amanlou M, Allen BJ. Biodistribution of ultra-small superparamagnetic iron oxide nanoparticles in BALB mice. *J Radioanal Nucl Chem.* 2013; 295: 1517-23.
- Shanehsazzadeh S, Oghabian MA, Lahooti A, Abdollahi M, Haeri SA, Amanlou M, et al. Estimated background doses of [<sup>67</sup>Ga]-DTPA-USPIO in normal Balb/c mice as a potential therapeutic agent for liver and spleen cancers. *Nucl Med Commun.* 2013; 34: 915-25.

51. de Rosales RTM, Tavaré R, Glaria A, Varma G, Protti A, Blower PJ. <sup>99m</sup>Tc-bisphosphonate-iron oxide nanoparticle conjugates for dual-modality biomedical imaging. *Bioconjugate Chem.* 2011; 22: 455-65.
52. Sandiford L, Phinikaridou A, Protti A, Meszaros LK, Cui X, Yan Y, et al. Bisphosphonate-anchored PEGylation and radiolabeling of superparamagnetic iron oxide: long-circulating nanoparticles for in vivo multimodal (T1 MRI-SPECT) imaging. *ACS Nano.* 2013; 7: 500-12.
53. Sandiford L, de Rosales RTM. The use of contrast agents in clinical and preclinical PET-MR imaging. *PET Clin.* 2016; 11: 119-128.
54. Lee CM, Jeong HJ, Kim EM, Kim DW, Lim ST, Kim HT, et al. Superparamagnetic iron oxide nanoparticles as a dual imaging probe for targeting hepatocytes in vivo. *Magn Reson Med.* 2009; 62: 1440-6.
55. Tu C, Ng TS, Jacobs RE, Louie AY. Multimodality PET/MRI agents targeted to activated macrophages. *J Biol Inorg Chem.* 2014; 19: 247-58.
56. Jarrett BR, Correa C, Ma KL, Louie AY. In vivo mapping of vascular inflammation using multimodal imaging. *PLoS One.* 2010; 5: e13254.
57. Kim SM, Chae MK, Yim MS, Jeong IH, Cho J, Lee C, et al. Hybrid PET/MR imaging of tumors using an oleanolic acid-conjugated nanoparticle. *Biomaterials.* 2013; 34: 8114-21.
58. Moon SH, Yang BY, Kim YJ, Hong MK, Lee YS, Lee DS, et al. Development of a complementary PET/MR dual-modal imaging probe for targeting prostate-specific membrane antigen (PSMA). *Nanomedicine.* 2016; 12: 871-9.
59. Shانهsazzadeh S, Gruettner C, Lahouti A, Mahmoudi M, Allen BJ, Ghavami M, et al. Monoclonal antibody conjugated magnetic nanoparticles could target MUC-1-positive cells in vitro but not in vivo. *Contrast Media Mol Imaging.* 2015; 10: 225-36.
60. Sharma R, Xu Y, Kim SW, Schueller MJ, Alexoff D, Smith SD, et al. Carbon-11 radiolabeling of iron-oxide nanoparticles for dual-modality PET/MR imaging. *Nanoscale.* 2013; 5: 7476-83.
61. Zhu J, Zhang B, Tian J, Wang J, Chong Y, Wang X, et al. Synthesis of heterodimer radionuclide nanoparticles for magnetic resonance and single-photon emission computed tomography dual-modality imaging. *Nanoscale.* 2015; 7: 3392-5.
62. Thorek DLJ, Ulmert D, Diop NFM, Lupu ME, Doran MG, Huang RM, et al. Non-invasive mapping of deep-tissue lymph nodes in live animals using a multimodal PET/MRI nanoparticle. *Nat Commun.* 2014; 5: 3097.
63. Heuveling DA, Visser GW, Baclayon M, Roos WH, Wuite GJ, Hoekstra OS, et al. <sup>89</sup>Zr-nanocolloidal albumin-based PET/CT lymphoscintigraphy for sentinel node detection in head and neck cancer: Preclinical results. *J Nucl Med.* 2011; 52: 1580-4.
64. Heuveling DA, van Schie A, Vugts DJ, Hendrikse NH, Yaqub M, Hoekstra OS, et al. Pilot study on the feasibility of PET/CT lymphoscintigraphy with <sup>89</sup>Zr-nanocolloidal albumin for sentinel node identification in oral cancer patients. *J Nucl Med.* 2013; 54: 585-9.
65. Wong RM, Gilbert DA, Liu K, Louie AY. Rapid size-controlled synthesis of dextran-coated, <sup>64</sup>Cu-doped iron oxide nanoparticles. *ACS Nano.* 2012; 6: 3461-7.
66. Boros E, Bowen AM, Josephson L, Vasdev N, Holland JP. Chelate-free metal ion binding and heat-induced radiolabeling of iron oxide nanoparticles. *Chem Sci.* 2015; 6: 225-36.
67. Yuan H, Wilks MQ, Normandin MD, El Fakhri G, Kaittani C, Josephson L. Heat-induced radiolabeling and fluorescence labeling of Feraheme nanoparticles for PET/SPECT imaging and flow cytometry. *Nat Protoc.* 2018; 13: 392-412.
68. Yuan H, Wilks MQ, El Fakhri G, Normandin MD, Kaittani C, Josephson L. Heat-induced-radiolabeling and click chemistry: A powerful combination for generating multifunctional nanomaterials. *PLoS One.* 2017; 12: e0172722.
69. Normandin MD, Yuan H, Wilks MQ, Chen HH, Kinsella JM, Cho H, et al. Heat-induced radiolabeling of nanoparticles for monocyte tracking by PET. *Angew Chem Int Ed.* 2015; 54: 13002-6.
70. Sirbulescu RF, Boehm CK, Soon E, Wilks MQ, Ilies I, Yuan H, et al. Mature B cells accelerate wound healing after acute and chronic diabetic skin lesions. *Wound Rep Reg.* 2017; 25: 774-91.
71. Pellico J, Ruiz-Cabello J, Saiz-Alfía M, Rosario G, Caja S, Montoya M, et al. Fast synthesis and bioconjugation of <sup>68</sup>Ga core-doped extremely small iron oxide nanoparticles for PET/MR imaging. *Contrast Media Mol Imaging.* 2016; 11: 203-10.
72. Chen F, Ellison PA, Lewis CM, Hong H, Zhang Y, Shi S, et al. Chelator-free synthesis of a dual-modality PET/MRI agent. *Angew Chem Int Ed.* 2013; 52: 13319-23.
73. Pham TN, Lengkeek NA, Greguric I, Kim BJ, Pellegrini PA, Bickley SA, et al. Tunable and noncytotoxic PET/SPECT-MRI multimodality imaging probes using colloiddally stable ligand-free superparamagnetic iron oxide nanoparticles. *Int J Nanomedicine.* 2017; 12: 899-909.
74. Chakravarty R, Valdovinos HF, Chen F, Lewis CM, Ellison PA, Luo H, et al. Intrinsically germanium-69-labeled iron oxide nanoparticles: synthesis and in-vivo dual-modality PET/MR imaging. *Adv Mater.* 2014; 26: 5119-23.
75. Freund B, Tromsdorf UJ, Bruns OT, Heine M, Giemsa A, Bartelt A, et al. A simple and widely applicable method to <sup>59</sup>Fe-radiolabel monodisperse superparamagnetic iron oxide nanoparticles for in vivo quantification studies. *ACS Nano.* 2012; 6: 7318-25.
76. Liu Z, Tabakman S, Welscher K, Dai H. Carbon nanotubes in biology and medicine: In vitro and in vivo detection, imaging and drug delivery. *Nano Res.* 2009; 2: 85-120.
77. Wang JTW, Fabbro C, Venturelli E, Menard-Moyon C, Chaloin O, Da Ros T, et al. The relationship between the diameter of chemically-functionalized multi-walled carbon nanotubes and their organ biodistribution, profiles in vivo. *Biomaterials.* 2014; 35: 9517-28.
78. Liu Z, Cai W, He L, Nakayama N, Chen K, Sun X, et al. In vivo biodistribution and highly efficient tumour targeting of carbon nanotubes in mice. *Nat Nanotechnol.* 2007; 2: 47-52.
79. McDewitt MR, Chattopadhyay D, Kappel BJ, Jaggi JS, Schiffman SR, Antczak C, et al. Tumor targeting with antibody-functionalized, radiolabeled carbon nanotubes. *J Nucl Med.* 2007; 48: 1180-9.
80. Tran LA, Hernández-Rivera M, Berlin AN, Zheng Y, Sampaio L, Bovee C, et al. The use of gadolinium-carbon nanostructures to magnetically enhance stem cell retention for cellular cardiomyoplasty. *Biomaterials.* 2014; 35: 720-6.
81. Lamanna G, Garofalo A, Popa G, Wilhelm C, Bégin-Colin S, Felder-Flesch D, et al. Endowing carbon nanotubes with superparamagnetic properties: applications for cell labeling, MRI cell tracking and magnetic manipulations. *Nanoscale.* 2013; 5: 4412-21.
82. Liu Y, Hughes TC, Muir BW, Waddington LJ, Gengenbach TR, Easton CD, et al. Water-dispersible magnetic carbon nanotubes as T2-weighted MRI contrast agents. *Biomaterials.* 2014; 35: 378-86.
83. Wang JTW, Cabana L, Bourgognon M, Kafa H, Protti A, Venner K, et al. Magnetically decorated multiwalled carbon nanotubes as dual MRI and SPECT contrast agents. *Adv Funct Mater.* 2014; 24: 1880-94.
84. Cabana L, Bourgognon M, Wang JTW, Protti A, Klippstein R, de Rosales RTM, et al. The shortening of MWNT-SPION hybrids by steam treatment improves their magnetic resonance imaging properties in vitro and in vivo. *Small.* 2016; 12: 2893-905.
85. Truillet C, Bouziotis P, Tsoukalas C, Brugière J, Martini M, Sancey L, et al. Ultrasmall particles for Gd-MRI and <sup>68</sup>Ga-PET dual imaging. *Contrast Media Mol Imaging.* 2015; 10: 309-19.
86. Mignot A, Truillet C, Lux F, Sancey L, Louis C, Denat F, et al. A top-down synthesis route to ultrasmall multifunctional Gd-based silica nanoparticles for theranostic applications. *Chem Eur J.* 2013; 19: 6122-36.
87. Lux F, Mignot A, Mowat P, Louis C, Dufort S, Bernhard C, et al. Ultrasmall rigid particles as multimodal probes for medical applications. *Angew Chem Int Ed.* 2011; 50: 12299-303.
88. ElBayoumi TA, Torchilin VP. Tumor-targeted nanomedicines: enhanced antitumor efficacy in vivo of doxorubicin-loaded, long-circulating liposomes modified with cancer-specific monoclonal antibody. *Clin Cancer Res.* 2009; 15: 1973-80.
89. Iwase Y, Maitani Y. Octreotide-targeted liposomes loaded with CPT-11 enhanced cytotoxicity for the treatment of medullary thyroid carcinoma. *Mol Pharm.* 2011; 8: 330-7.
90. Zielhuis SW, Seppenwoolde JH, Mateus VA, Bakker CJ, Krijger GC, Storm G, et al. Lanthanide-loaded liposomes for multimodality imaging and therapy. *Cancer Biother Radiopharm.* 2006; 21: 520-7.
91. Abou DS, Thorek DL, Ramos NN, Pinkse MWH, Wolterbeek HT, Carlin SD, et al. <sup>89</sup>Zr-labeled paramagnetic octreotide-liposomes for PET-MR imaging of cancer. *Pharm Res.* 2013; 30: 878-88.
92. Sirol M, Fuster V, Badimon JJ, Fallon JT, Moreno PR, Toussaint JF, et al. Chronic thrombus detection with in vivo magnetic resonance imaging and a fibrin-targeted contrast agent. *Circulation.* 2005; 112: 1594-600.
93. Uppal R, Ciesienki KL, Chonde DB, Loving GS, Caravan P. Discrete bimodal probes for thrombus imaging. *J Am Chem Soc.* 2012; 134: 10799-802.
94. Uppal R, Catana C, Ay I, Benner T, Sorensen AG, Caravan P. Bimodal thrombus imaging: simultaneous PET/MR imaging with a fibrin-targeted dual PET/MR probe—feasibility study in rat model. *Radiology.* 2011; 258: 812-20.
95. Lijowski M, Caruthers S, Hu G, Zhang H, Scott MJ, Williams T, et al. High sensitivity: high-resolution SPECT-CT/MR molecular imaging of angiogenesis in the Vx2 model. *Invest Radiol.* 2009; 44: 15-22.
96. Kim C, Favazza C, Wang LV. In vivo photoacoustic tomography of chemicals: high-resolution functional and molecular optical imaging at new depths. *Chem Rev.* 2010; 110: 2756-82.
97. Gros CP, Eggenspiller A, Nonat A, Barbe J-M, Denat F. New potential bimodal imaging contrast agents based on DOTA-like and porphyrin macrocycles. *MedChemComm.* 2011; 2: 119-25.
98. Ni Y. Metalloporphyrins and functional analogues as MRI contrast agents. *Curr Med Imaging Rev.* 2008; 4: 96-112.
99. Foster C, Woo DV, Kaltovich F, Emrich J, Ljungquist C. Delineation of a transplanted malignant melanoma with indium-111-labeled porphyrin. *J Nucl Med.* 1985; 26: 756-60.
100. Fan Q, Cheng K, Hu X, Ma X, Zhang R, Yang M, et al. Transferring biomarker into molecular probe: melanin nanoparticle as a naturally active platform for multimodality imaging. *J Am Chem Soc.* 2014; 136: 15185-94.
101. Yang M, Fan Q, Zhang R, Cheng K, Yan J, Pan D, et al. Dragon fruit-like biocage as an iron trapping nanopatform for high efficiency targeted cancer multimodality imaging. *Biomaterials.* 2015; 69: 30-7.
102. Lewin M, Carlesso N, Tung C-H, Tang X-W, Cory D, Scadden DT, et al. Tat peptide-derivatized magnetic nanoparticles allow in vivo tracking and recovery of progenitor cells. *Nat Biotechnol.* 2000; 18: 410-4.
103. Nahrendorf M, Zhang H, Hembador S, Panizzi P, Sosnovik DE, Aikawa E, et al. Nanoparticle PET-CT imaging of macrophages in inflammatory atherosclerosis. *Circulation.* 2008; 117: 379-87.

104. Nahrendorf M, Keliher E, Marinelli B, Leuschner F, Robbins CS, Gerszten RE, et al. Detection of macrophages in aortic aneurysms by nanoparticle positron emission tomography-computed tomography. *Arterioscler Thromb Vasc Biol.* 2011; 31: 750-7.
105. Steller L, Pinkernelle JG, Michel R, Schwartlander R, Raschzok N, Morgul MH, et al. Modification of aminosilanized superparamagnetic nanoparticles: Feasibility of multimodal detection using 3T MRI, small animal PET, and fluorescence imaging. *Mol Imaging Biol.* 2010; 12: 25-34.
106. Xie J, Chen K, Huang J, Lee S, Wang J, Gao J, et al. PET/NIRF/MRI triple functional iron oxide nanoparticles. *Biomaterials.* 2010; 31: 3016-22.
107. Park JC, Yu MK, An GI, Park S-I, Oh J, Kim HJ, et al. Facile preparation of a hybrid nanoprobe for triple-modality optical/PET/MR imaging. *Small.* 2010; 6: 2863-8.
108. Madru R, Tran TA, Axelsson J, Ingvar C, Bibic A, Ståhlberg F, et al. <sup>68</sup>Ga-labeled superparamagnetic iron oxide nanoparticles (SPIONs) for multi-modality PET/MR/Cherenkov luminescence imaging of sentinel lymph nodes. *Am J Nucl Med Mol Imaging.* 2014; 4: 60-69.
109. Kim JS, Kim Y-H, Kim JH, Kang KW, Tae EL, Youn H, et al. Development and in vivo imaging of a PET/MRI nanoprobe with enhanced NIR fluorescence by dye encapsulation. *Nanomedicine (Lond).* 2012; 7: 219-29.
110. Kobayashi H, Kawamoto S, Bernardo M, Brechbiel MW, Knopp MV, Choyke PL. Delivery of gadolinium-labeled nanoparticles to the sentinel lymph node: comparison of the sentinel node visualization and estimations of intra-nodal gadolinium concentration by the magnetic resonance imaging. *J Control Release.* 2006; 111: 343-51.
111. Nakajima M, Takeda M, Kobayashi M, Suzuki S, Ohuchi N. Nano-sized fluorescent particles as new tracers for sentinel node detection: experimental model for decision of appropriate size and wavelength. *Cancer Sci.* 2005; 96: 353-6.
112. Hwang DW, Ko HY, Lee JH, Kang H, Ryu SH, Song IC, et al. A nucleolin-targeted multimodal nanoparticle imaging probe for tracking cancer cells using an aptamer. *J Nucl Med.* 2010; 51: 98-105.
113. Wang C, Xu C, Zeng H, Sun S. Recent progress in syntheses and applications of dumbbell-like nanoparticles. *Adv Mater.* 2009; 21: 3045-52.
114. Xu C, Xie J, Ho D, Wang C, Kohler N, Walsh EG, et al. Au-Fe<sub>3</sub>O<sub>4</sub> dumbbell nanoparticles as dual-functional probes. *Angew Chem Int Ed.* 2008; 47: 173-6.
115. Yu H, Chen M, Rice PM, Wang SX, White RL, Sun S. Dumbbell-like bifunctional Au-Fe<sub>3</sub>O<sub>4</sub> nanoparticles. *Nano Lett.* 2005; 5: 379-82.
116. Yang M, Cheng K, Qi S, Liu H, Jiang Y, Jiang H, et al. Affibody modified and radiolabeled gold-iron oxide hetero-nanostructures for tumor PET, optical and MR imaging. *Biomaterials.* 2013; 34: 2796-806.
117. Jin Q, Zhu W, Jiang D, Zhang R, Kuttyreff CJ, Engle JW, et al. Ultra-small iron-gallic acid coordination polymer nanoparticles for chelator-free labeling of <sup>64</sup>Cu and multimodal imaging-guided photothermal therapy. *Nanoscale.* 2017; 9: 12609-17.
118. Kumar R, Nyk M, Ohulchanskyy TY, Flask CA, Prasad PN. Combined optical and MR bioimaging using rare earth ion doped NaYF<sub>4</sub> nanocrystals. *Adv Funct Mater.* 2009; 19: 853-9.
119. Park YI, Kim JH, Lee KT, Jeon KS, Bin Na H, Yu JH, et al. Nonblinking and nonbleaching upconverting nanoparticles as an optical imaging nanoprobe and T1 magnetic resonance imaging contrast agent. *Adv Mater.* 2009; 21: 4467-71.
120. Zhou J, Sun Y, Du X, Xiong L, Hu H, Li F. Dual-modality in vivo imaging using rare-earth nanocrystals with near-infrared to near-infrared (NIR-to-NIR) upconversion luminescence and magnetic resonance properties. *Biomaterials.* 2010; 31: 3287-95.
121. Hu H, Li D, Liu S, Wang M, Moats R, Conti PS, et al. Integrin αβ<sub>3</sub> targeted GdVO<sub>4</sub>:Eu ultrathin nanosheet for multimodal PET/MR imaging. *Biomaterials.* 2014; 35: 8649-58.
122. Huang X, Zhang F, Lee S, Swierczewska M, Kiesewetter DO, Lang L, et al. Long-term multimodal imaging of tumor draining sentinel lymph nodes using mesoporous silica-based nanoprobes. *Biomaterials.* 2012; 33: 4370-8.
123. Zhou J, Yu M, Sun Y, Zhang X, Zhu X, Wu Z, et al. Fluorine-18-labeled Gd<sup>3+</sup>/Yb<sup>3+</sup>/Er<sup>3+</sup> co-doped NaYF<sub>4</sub> nanophosphors for multimodality PET/MR/UCL imaging. *Biomaterials.* 2011; 32: 1148-56.
124. Lee J, Lee TS, Ryu J, Hong S, Kang M, Im K, et al. RGD peptide-conjugated multimodal NaGdF<sub>4</sub>:Yb<sup>3+</sup>/Er<sup>3+</sup> nanophosphors for upconversion luminescence, MR, and PET imaging of tumor angiogenesis. *J Nucl Med.* 2013; 54: 96-103.
125. Zhong C, Yang P, Li X, Li C, Wang D, Gai S, et al. Monodisperse bifunctional Fe<sub>3</sub>O<sub>4</sub>@NaGdF<sub>4</sub>:Yb/Er@NaGdF<sub>4</sub>:Yb/Er core-shell nanoparticles. *RSC Advances.* 2012; 2: 3194-7.
126. Xia A, Gao Y, Zhou J, Li C, Yang T, Wu D, et al. Core-shell NaYF<sub>4</sub>:Yb<sup>3+</sup>, Tm<sup>3+</sup>@Fe<sub>3</sub>O<sub>4</sub> nanocrystals for dual-modality T2-enhanced magnetic resonance and NIR-to-NIR upconversion luminescent imaging of small-animal lymphatic node. *Biomaterials.* 2011; 32: 7200-8.
127. He H, Xie MY, Ding Y, Yu XF. Synthesis of Fe<sub>3</sub>O<sub>4</sub>@LaF<sub>3</sub>:Ce,Tb nanocomposites with bright fluorescence and strong magnetism. *Appl Surf Sci.* 2009; 255: 4623-6.
128. Cui X, Mathe D, Kovács Nm, Horváth I, Jauregui-Osoro M, de Rosales RTM, et al. Synthesis, characterization, and application of core-shell Co<sub>0.16</sub>Fe<sub>2.84</sub>O<sub>4</sub>@NaYF<sub>4</sub>(Yb, Er) and Fe<sub>3</sub>O<sub>4</sub>@NaYF<sub>4</sub>(Yb,Tm) nanoparticle as Trimodal (MRI, PET/SPECT, and optical) imaging agents. *Bioconjugate Chem.* 2016; 27: 319-28.
129. Lin X, Xie J, Niu G, Zhang F, Gao H, Yang M, et al. Chimeric ferritin nanocages for multiple function loading and multimodal imaging. *Nano Lett.* 2011; 11: 814-9.
130. Sakulkhu U, Mahmoudi M, Maurizi L, Salaklang J, Hofmann H. Protein corona composition of superparamagnetic iron oxide nanoparticles with various physico-chemical properties and coatings. *Sci Rep.* 2014; 4: 5020.
131. Li SD, Huang L. Pharmacokinetics and biodistribution of nanoparticles. *Mol Pharm.* 2008; 5: 496-504.
132. Desai MP, Labhasetwar V, Amidon GL, Levy RJ. Gastrointestinal uptake of biodegradable microparticles: effect of particle size. *Pharm Res.* 1996; 13: 1838-45.
133. Bumb A, Regino CAS, Egen JG, Bernardo M, Dobson PJ, Germain RN, et al. Trafficking of a dual-modality magnetic resonance and fluorescence imaging superparamagnetic iron oxide-based nanoprobe to lymph nodes. *Mol Imaging Biol.* 2011; 13: 1163-72.
134. Reddy ST, Rehor A, Schmoekel HG, Hubbell JA, Swartz MA. In vivo targeting of dendritic cells in lymph nodes with poly(propylene sulfide) nanoparticles. *J Control Release.* 2006; 112: 26-34.
135. Cutler CS, Hennkens HM, Sisay N, Huclier-Markai S, Jurisson SS. Radiometals for combined imaging and therapy. *Chem Rev.* 2013; 113: 858-83.
136. De Silva RA, Jain S, Lears KA, Chong H-S, Kang CS, Sun X, et al. Copper-64 radiolabeling and biological evaluation of bifunctional chelators for radiopharmaceutical development. *Nucl Med Biol.* 2012; 39: 1099-104.
137. Liu Y, Welch MJ. Nanoparticles labeled with positron emitting nuclides: advantages, methods, and applications. *Bioconjugate Chem.* 2012; 23: 671-82.
138. Wadas TJ, Wong EH, Weisman GR, Anderson CJ. Coordinating radiometals of copper, gallium, indium, yttrium, and zirconium for PET and SPECT imaging of disease. *Chem Rev.* 2010; 110: 2858-902.
139. Wang Y, Liu Y, Luehmann H, Xia X, Brown P, Jarreau C, et al. Evaluating the pharmacokinetics and in vivo cancer targeting capability of Au nanocages by positron emission tomography imaging. *ACS Nano.* 2012; 6: 5880-8.
140. Holland JP, Williamson MJ, Lewis JS. Unconventional nuclides for radiopharmaceuticals. *Mol Imaging.* 2010; 9: 1-20.
141. Fang J, Nakamura H, Maeda H. The EPR effect: Unique features of tumor blood vessels for drug delivery, factors involved, and limitations and augmentation of the effect. *Adv Drug Deliv Rev.* 2011; 63: 136-51.
142. Zhao F, Zhao Y, Liu Y, Chang X, Chen C, Zhao Y. Cellular uptake, intracellular trafficking, and cytotoxicity of nanomaterials. *Small.* 2011; 7: 1322-37.
143. Harisinghani MG, Barentsz J, Hahn PF, Deserno WM, Tabatabaei S, van de Kaa CH, et al. Noninvasive detection of clinically occult lymph-node metastases in prostate cancer. *N Engl J Med.* 2003; 348: 2491-9.